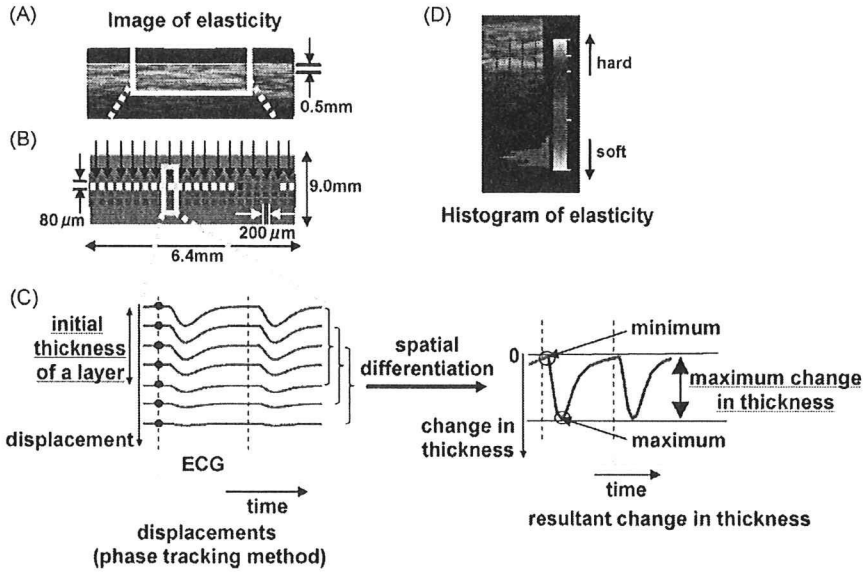

Fig. 1. Evaluation of carotid artery elasticity by phase tracking method. Arterial elasticity is displayed as a 2D cross-sectional color image, which is updated at every heartbeat (A). Multiple sites are preset from the luminal surface to the adventitia (113 depths × 32 beams per 9 mm × 6.4 mm scanned area) and elasticity in each module is measured by the phase tracking method (B). The arterial wall was divided into multiple layers with thicknesses set at 320 μm. The changes in thickness at each depth during the cardiac cycle are simultaneously obtained, and the maximum change in thickness corresponds to the elasticity in each module (C). The elasticity distribution is shown as a histogram (D).

1.6. Statistical analysis

Variables were compared using Pearson's regression analysis. Then, a multiple linear regression analysis was performed to evaluate the independent parameters that were significantly related to arterial elasticity. All data are expressed means ± S.D., and a p-value less than 0.05 was accepted as indicating statistical significance. All statistical analyses were performed using the Statistical Package for the Social Sciences version 13.0 (SPSS Japan Inc., Tokyo, Japan).

2. Results

The clinical characteristics of 78 subjects are shown in Table 1. Mean age is 41.0 ± 13.9 years, BMI 37.6 ± 7.2 (kg/m^2). Thus, the subjects were relatively young and categorized as having moderate, extreme or severe obesity according to Japanese guidelines.

To assess the clinical relevance of carotid artery elasticity in obese subjects, the arterial elasticity value was compared to atherosclerosis values obtained with currently established methods, carotid IMT and PWV. Arterial elasticity showed significant positive correlations with both carotid IMT (r = 0.422, p < 0.01) and PWV (r = 0.360, p < 0.01) in obese subjects (Fig. 2). Similar positive correlations among these three atherosclerosis values were observed in our previous results in subjects with type 2 diabetes [21]. The IMT value in this study was 0.61 ± 0.17 (range: 0.30–1.20) mm and PWV was 1396 ± 260 (range: 992–2117) cm/s, i.e. these obese subjects did not have advanced atherosclerosis, in contrast to the results in subjects with type 2 diabetes in our previous study (IMT: 0.94 ± 0.30 mm, PWV: 1703 ± 356 cm/s).

We then explored the association of carotid arterial elasticity with the clinical and demographic characteristics of these obese

Table 1
Subject characteristics.

Number	78
Age, years	41.0 ± 13.9
Gender (male), %	29.5
Body weight, kg	98.8 ± 24.2
BMI, kg/m^2	37.6 ± 7.2
Fasting blood glucose, mg/dl	121.3 ± 47.6
HbA1c, %	6.5 ± 1.8
Serum insulin μU/ml	17.8 ± 13.2
HOMA-R	4.5 ± 3.8
Systolic BP, mmHg	126.9 ± 14.4
Diastolic BP, mmHg	79.8 ± 10.7
Total cholesterol, mg/dl	208.2 ± 43.5
HDL cholesterol, mg/dl	45.8 ± 9.6
LDL cholesterol, mg/dl	132.6 ± 32.9
Triglyceride, mg/dl	184.1 ± 177.4
Uric acid, mg/dl	5.9 ± 1.5
Visceral fat area, cm^2	150.3 ± 55.7
Subcutaneous fat area, cm^2	405.7 ± 160.0
Diabetes, %	46.8
Dyslipidemia, %	60.3
Hypertension, %	48.7
Current smoker, %	28.0

Mean ± S.D.

Table 2
Associations between atherosclerosis values and subject characteristics.

Variables	r		
	Elasticity	IMT	PWV
Age	0.46**	0.44**	0.67**
Male	0.27*	0.24**	−0.086
Body weight	0.03	−0.075	−0.11
BMI	0.07	−0.06	0.045
Fasting blood glucose	0.14	0.032	0.14
HbA1c	−0.02	−0.036	0.0095
Total cholesterol	0.20	0.061	0.030
HDL cholesterol	−0.03	0.19	0.060
LDL cholesterol	0.15	0.034	−0.049
Triglyceride	−0.03	0.005	−0.040
Systolic BP	0.38**	0.27*	0.35**
Diastolic BP	0.28*	0.26*	0.047
Uric acid	0.15	0.10	−0.20
Diabetes	0.15	0.091	0.39**
Dyslipidemia	0.04	−0.11	0.037
Hypertension	0.37**	0.39**	0.51**

* p < 0.05.
** p < 0.01.

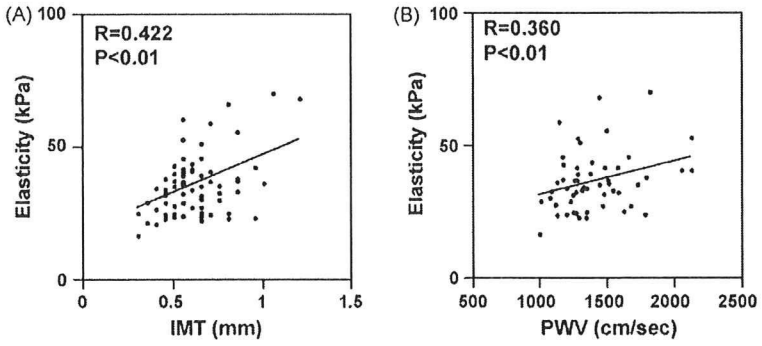

Fig. 2. Correlations of arterial elasticity with carotid IMT (A) and PWV (B) in obese subjects.

Table 3
Associations between each atherosclerosis value and fat distribution.

Variables	r		
	Elasticity	IMT	PWV
Visceral fat area	0.42**	0.25*	0.31*
Subcutaneous fat area	−0.066	−0.111	0.046

* $p<0.05$.
** $p<0.01$.

Table 5
Multivariate adjustment for parameters related to visceral fat area.

Variables	Regression coefficient	p
Elasticity	0.34	0.0041
IMT	0.034	0.77
PWV	0.22	0.047

$R^2 = 0.23$.

subjects. As shown in Table 2, arterial elasticity correlated with age ($r=0.46$, $p<0.01$), gender ($r=0.27$, $p<0.05$), BP, both systolic ($r=0.38$, $p<0.01$) and diastolic ($r=0.28$, $p<0.05$), and hypertension ($r=0.37$, $p<0.01$). Carotid IMT and PWV also showed similar associations with age, systolic BP and hypertension.

To evaluate whether fat distribution affects atherosclerosis in obese subjects, we performed a single regression analysis of atherosclerosis values with subcutaneous or visceral fat accumulation, as determined by CT scanning. Interestingly, visceral fat area correlated significantly with arterial elasticity as well as carotid IMT and PWV (Table 3), whereas subcutaneous fat area showed no apparent association with these three atherosclerosis values in the present study. Then, we performed multiple linear regression analysis with parameters related to atherosclerosis values, i.e. age, hypertension and visceral fat area (Tables 2 and 3), to search for independent variables affecting atherosclerosis values in obese subjects. As shown in Table 4, each atherosclerosis value is associated with age, indicating that age is also a strong atherosclerosis determinant in obese subjects. Intriguingly, the analysis revealed that visceral fat area is an independent variable showing a positive correlation with carotid arterial elasticity, but not carotid IMT or PWV. We next analyzed the results in a different way, to determine which of the atherosclerosis values is most strongly associated with visceral adiposity. Visceral fat area was significantly associated with both arterial elasticity and PWV, though the correlation with arterial elasticity was stronger (Table 5). These results suggest that arterial elasticity is an excellent parameter of atherosclerosis as compared with currently established atherosclerosis values and might reflect the cardiovascular risk of visceral adiposity.

Table 4
Multivariate adjustment for parameters related to atherosclerosis values.

Variables	Regression coefficient		
	Elasticity[a]	IMT[b]	PWV[c]
Age	0.30*	0.34**	0.52**
Visceral fat area	0.28**	0.075	−0.06
Hypertension	0.13	0.019	0.32*

[a] $R^2 = 0.32$.
[b] $R^2 = 0.25$.
[c] $R^2 = 0.47$.
* $p<0.05$
** $p<0.01$.

3. Discussion

We measured two established atherosclerosis values, carotid IMT and PWV, in addition to "arterial elasticity", which was measured by a novel method, in this study. Similar to our previous results in subjects with type 2 diabetes [21], the arterial elasticity value was significantly associated with those of carotid IMT and PWV. These results raise the possibility of evaluating atherosclerosis in obese subjects with this novel method of measuring elasticity. The important finding of the present study is that arterial elasticity is a better measurement than either carotid IMT or PWV for evaluating the effect of visceral fat accumulation on atherosclerosis in obese subjects; the multiple linear regression analysis revealed that only carotid arterial elasticity, not carotid IMT or PWV, showed a positive correlation with visceral fat area.

In addition, our present results clearly shows that visceral adiposity rather than subcutaneous adiposity is an important factor affecting atherosclerosis in Japanese obese subjects with BMI over 30, since all three parameters for evaluating atherosclerosis, arterial elasticity, carotid IMT and PWV, were significantly associated with visceral fat area but not with subcutaneous fat area. Abdominal fat accumulation, especially visceral adiposity, is well known to play a crucial role in the development of metabolic syndrome [26], leading to atherosclerosis and ultimately cardiovascular disease [6]. Indeed, visceral adiposity determined by CT scanning was related to the incidence of coronary artery disease [8]. Furthermore, recent reports have shown several surrogate markers for atherosclerosis, such as carotid IMT [9–13] and arterial stiffness [15], to be associated with intra-abdominal fat accumulation in subjects without advanced atherosclerosis. Since obesity is increasing explosively world-wide, a practical and non-invasive method is urgently needed for early detection of atherosclerosis before serious cardiovascular events occur.

Herein, we have shown that our novel method of measuring arterial elasticity has potential for detecting early stage atherosclerosis in obese subjects. This ultrasonic method accurately tracks arterial wall movements based on both the phase and the

magnitude of demodulated signals, allowing instantaneous determination of the position of an object. With this method, it is possible to accurately detect small-amplitude velocity signals, less than a few micrometers, which are superimposed on arterial motion due to the heartbeat. Thus, the values obtained with this method reflect an important characteristic of vessel walls, i.e. arterial elasticity. We previously reported arterial elasticity to be a promising method of evaluating early stage atherosclerosis in subjects with type 2 diabetes [21]. Taken together with the present results in obese subjects, these finding indicate that measurement of arterial elasticity might be broadly applicable to evaluation of subjects with atherosclerosis-prone metabolic disorders.

This novel method also has potential for evaluating the elasticity distribution in vessel walls with high spatial resolution; the elasticity distribution is demonstrated as a histogram as shown in Fig. 1D. Properties of the histogram, such as deviation and the shape of the distribution, which were not used in this study, would provide additional information regarding qualitative changes in atherosclerosis. This possibility should be pursued in future investigations.

Several studies have examined which obesity-related values, including body weight, BMI, waist–hip ratio and abdominal fat accumulation, are closely associated with atherosclerosis values such as carotid IMT [27,28] and PWV [29]. However, comparisons among these atherosclerosis values were not conducted, i.e., which of the atherosclerosis values, IMT, PWV or elasticity, is most strongly associated with obesity-related values remains to be determined. This is the first report demonstrating arterial elasticity to have a stronger association with visceral fat area in obese subjects than the two most widely used atherosclerosis values, IMT and PWV.

The present study has several limitations. The study design was cross-sectional. Determination of whether arterial elasticity predicts cardiovascular events in the future thus awaits a prospective study. Another issue warranting further investigation is whether reducing visceral adiposity would improve arterial elasticity. Another important issue is that only approximately 30% of our study subjects were male. The difference in fat distribution by gender is well known, i.e. visceral adiposity is more frequently observed in males [30] and subcutaneous adiposity in females [25]. However, despite the female dominance in our subject group, the effect of visceral adiposity on arterial elasticity was confirmed by multiple regression analysis, implying a crucial role of visceral fat in atherosclerosis.

In conclusion, the present results indicate that arterial elasticity is a novel, sensitive parameter for evaluating atherosclerosis in obese subjects, potentially more useful than currently established atherosclerosis values. Measuring arterial elasticity hold promise of detecting minute vascular changes in early stage atherosclerosis, and may have broad clinical applications for evaluating atherosclerosis in subjects with metabolic disorders.

Acknowledgments

This work was supported by a Grant-in-Aid for Scientific Research (19591031) to Y. Ishigaki and the Global-COE Programs to Y. Oka from the Ministry of Education, Culture, Sports, Science and Technology of Japan. This work was also supported by a Grant-in-Aid for Research on Human Genome, Tissue Engineering (H17-genome-003) to Y. Oka. We thank Dr. T. Ohkubo for helpful suggestions on the statistical analysis. We also thank N. Tamura for technical support.

References

[1] Friedman JM. A war on obesity, not the obese. Science 2003;299:856–8.
[2] Yusuf S, Hawken S, Ounpuu S, et al. Obesity and the risk of myocardial infarction in 27,000 participants from 52 countries: a case-control study. Lancet 2005;366:1640–9.
[3] Eckel RH, Grundy SM, Zimmet PZ. The metabolic syndrome. Lancet 2005;365:1415–28.
[4] Klein S, Burke LE, Bray GA, et al. Clinical implications of obesity with specific focus on cardiovascular disease: a statement for professionals from the American Heart Association Council on Nutrition, Physical Activity, and Metabolism: endorsed by the American College of Cardiology Foundation. Circulation 2004;110:2952–67.
[5] Poirier P, Eckel RH. Obesity and cardiovascular disease. Curr Atheroscler Rep 2002;4:448–53.
[6] Matsuzawa Y. Therapy Insight: adipocytokines in metabolic syndrome and related cardiovascular disease. Nat Clin Pract Cardiovasc Med 2006;3:35–42.
[7] Fujioka S, Matsuzawa Y, Tokunaga K, Tarui S. Contribution of intra-abdominal fat accumulation to the impairment of glucose and lipid metabolism in human obesity. Metabolism 1987;36:54–9.
[8] Nakamura T, Tokunaga K, Shimomura I, et al. Contribution of visceral fat accumulation to the development of coronary artery disease in non-obese men. Atherosclerosis 1994;107:239–46.
[9] Yamamoto M, Egusa G, Hara H, Yamakido M. Association of intraabdominal fat and carotid atherosclerosis in non-obese middle-aged men with normal glucose tolerance. Int J Obes Relat Metab Disord 1997;21:948–51.
[10] Kim SK, Kim HJ, Hur KY, et al. Visceral fat thickness measured by ultrasonography can estimate not only visceral obesity but also risks of cardiovascular and metabolic diseases. Am J Clin Nutr 2004;79:593–9.
[11] Liu KH, Chan YL, Chan JC, Chan WB. Association of carotid intima–media thickness with mesenteric, preperitoneal and subcutaneous fat thickness. Atherosclerosis 2005;179:299–304.
[12] Lear SA, Humphries KH, Kohli S, Frohlich JJ, Birmingham CL, Mancini GB. Visceral adipose tissue, a potential risk factor for carotid atherosclerosis: results of the Multicultural Community Health Assessment Trial (M-CHAT). Stroke 2007;38:2422–9.
[13] Kawamoto R, Ohtsuka N, Ninomiya D, Nakamura S. Association of obesity and visceral fat distribution with intima–media thickness of carotid arteries in middle-aged and older persons. Intern Med 2008;47:143–9.
[14] Snell-Bergeon JK, Hokanson JE, Kinney GL, et al. Measurement of abdominal fat by CT compared to waist circumference and BMI in explaining the presence of coronary calcium. Int J Obes Relat Metab Disord 2004;28:1594–9.
[15] Sutton-Tyrrell K, Newman A, Simonsick EM, et al. Aortic stiffness is associated with visceral adiposity in older adults enrolled in the study of health, aging, and body composition. Hypertension 2001;38:429–33.
[16] Orr JS, Gentile CL, Davy BM, Davy KP. Large artery stiffening with weight gain in humans: role of visceral fat accumulation. Hypertension 2008;51:1519–24.
[17] Kanai H, Hasegawa H, Ichiki M, Tezuka F, Koiwa Y. Elasticity imaging of atheroma with transcutaneous ultrasound: preliminary study. Circulation 2003;107:3018–21.
[18] Hasegawa H, Kanai H, Hoshimiya N, Koiwa Y. Evaluating the regional elastic modules of a cylindeicl shell with nonuniform wall thickness. J Med Ultrason 2004;31:81–90.
[19] Kanai H, Sato M, Koiwa Y, Chubachi N. Transcutaneous measurement and spectrum analysis of heart wall vibrations. IEEE Trans Ultrason Ferroelectr Freq Control 1996;43:791–810.
[20] Kanai H, Koiwa Y, Zhang J. Real-time measurement of local myocardium motion and arterial wall thickening. IEEE Trans Ultrason Ferroelectr Freq Control 1999;46:1229–41.
[21] Okimoto H, Ishigaki Y, Koiwa Y, et al. A novel method for evaluating human carotid artery elasticity: possible detection of early stage atherosclerosis in subjects with type 2 diabetes. Atherosclerosis 2008;196:391–7.
[22] Hasegawa H, Kanai H, Hoshimiya N, Chubachi N, Koiwa Y. Accuracy evaluation in the measurement of a small change in the thickness of arterial walls and the measurement of elasticity of the human carotid artery. Jpn J Appl Phys 1998;37:3101–5.
[23] Sidhu PS, Desai SR. A simple and reproducible method for assessing intimal–medial thickness of the common carotid artery. Br J Radiol 1997;70:85–9.
[24] Munakata M, Ito N, Nunokawa T, Yoshinaga K. Utility of automated brachial ankle pulse wave velocity measurements in hypertensive patients. Am J Hypertens 2003;16:653–7.
[25] Kvist H, Sjostrom L, Tylen U. Adipose tissue volume determinations in women by computed tomography: technical considerations. Int J Obes 1986;10:53–67.
[26] Bjorntorp P. Metabolic implications of body fat distribution. Diabetes Care 1991;14:1132–43.
[27] Takami R, Takeda N, Hayashi M, et al. Body fatness and fat distribution as predictors of metabolic abnormalities and early carotid atherosclerosis. Diabetes Care 2001;24:1248–52.
[28] Ingelsson E, Sullivan LM, Fox CS, et al. Burden and prognostic importance of subclinical cardiovascular disease in overweight and obese individuals. Circulation 2007;116:375–84.
[29] Yamada J, Tomiyama H, Matsumoto C, et al. Overweight body mass index classification modifies arterial stiffening associated with weight gain in healthy middle-aged Japanese men. Hypertens Res 2008;31:1087–92.
[30] Kvist H, Chowdhury B, Sjostrom L, Tylen U, Cederblad A. Adipose tissue volume determination in males by computed tomography and 40K. Int J Obes 1988;12:249–66.

BRAIN RESEARCH 1263 (2009) 58–68

available at www.sciencedirect.com

ScienceDirect

www.elsevier.com/locate/brainres

BRAIN RESEARCH

Research Report

Obesity alters circadian expressions of molecular clock genes in the brainstem

Keizo Kaneko[a,b,1], Tetsuya Yamada[a,1], Sohei Tsukita[a,b], Kei Takahashi[a,b], Yasushi Ishigaki[a], Yoshitomo Oka[a,2], Hideki Katagiri[b,*,2]

[a]Division of Molecular Metabolism and Diabetes, Tohoku University Graduate School of Medicine, 2-1 Seiryo-machi, Aoba-ku, Sendai 980-8575, Japan

[b]Division of Advanced Therapeutics for Metabolic Diseases, Center for Translational and Advanced Animal Research, Tohoku University Graduate School of Medicine, 2-1 Seiryo-machi, Aoba-ku, Sendai 980-8575, Japan

ARTICLE INFO

Article history:
Accepted 30 December 2008
Available online 15 January 2009

Keywords:
Obesity
Insulin resistance
Circadian rhythm
Clock gene
Nucleus of the solitary tract
Metabolic syndrome

ABSTRACT

Major components of energy homeostasis, including feeding behavior and glucose and lipid metabolism, are subject to circadian rhythms. Recent studies have suggested that dysfunctions of molecular clock genes are involved in the development of obesity and diabetes. To examine whether metabolic states per se alter the circadian clock in the central nervous system (CNS), we analyzed the daily mRNA expression profiles of core clock genes in the caudal brainstem nucleus of the solitary tract (NTS). In lean C57BL/6 mice, transcript levels of the core clock genes (*Npas2*, *Bmal1*, *Per1*, *Per2* and *Rev-erbα*) clearly showed 24-h rhythmicity. On the other hand, the expression profiles of *Bmal1* and *Rev-erbα* were attenuated in mice with high fat diet-induced obesity as well as genetically obese KK-A^y and *ob/ob* mice. *Clock* expression levels were increased in mice with high fat diet-induced obesity and *Cry1* expression levels were decreased in KK-A^y and *ob/ob* mice. In addition, peroxisome proliferator-activated receptor α (PPARα), which reportedly increases the BMAL1 transcriptional level, was up-regulated in the NTS of these murine models of obesity and insulin resistance, suggesting involvement of PPARα in the attenuation of circadian rhythms in the NTS in obese states. Furthermore, a circadian expression profile of a downstream target of clock genes, the large conductance Ca^{2+}-activated K^+channel, was disturbed in the NTS of these murine obesity models. These perturbations might contribute to neuronal dysfunction in obese states. This is the first report showing that obesity perturbs the circadian expressions of core clock genes in the CNS.

1. Introduction

The worldwide prevalence of obesity and type 2 diabetes mellitus (T2DM) is increasing at an alarming rate, with major adverse consequences for human health (Flier, 2004). Since body weight and adiposity are maintained within a narrow range under steady state environmental conditions, the concept that a homeostatic center for energy metabolism

* *Corresponding author.* Fax: +81 22 717 8228.
E-mail address: katagiri@mail.tains.tohoku.ac.jp (H. Katagiri).
[1] Contributed equally.
[2] Contributed equally.

0006-8993/$ – see front matter © 2009 Published by Elsevier B.V.
doi:10.1016/j.brainres.2008.12.071

exists has been widely accepted and there is a growing consensus that this regulatory center is located mainly in the central nervous system (CNS), especially in the hypothalamus (Sandoval et al., 2008). Humoral factors, including insulin and adipokines, and afferent nerve signals (Uno et al., 2006); (Yamada et al., 2006) are known to be very important for conveying information regarding peripheral energy status to the CNS (Katagiri et al., 2007); (Yamada et al., 2008). We have proposed that the brain integrates and processes the peripheral metabolic information to send signals that control systemic metabolism (Katagiri et al., 2007).

Major components of energy homeostasis, such as feeding behavior and glucose and lipid metabolism, are subject to circadian rhythms. These rhythms are regulated by a circadian clock system composed of transcriptional/translational feedback loops that are now recognized to cycle in the suprachiasmatic nucleus (SCN) of the hypothalamus as well as in most peripheral tissues (Ramsey et al., 2007). In brief, each cell contains a set of core *clock* genes – *Clock*, *Bmal1*, *Cry* 1-2, *Per* 1-3 and nuclear receptors (*Rev-erbα*, *ROR*). The CLOCK/BMAL1 heterodimer regulates the production of proteins such as PER and CRY, which in turn regulate the production of BMAL1 (Schibler and Sassone-Corsi, 2002). Through these feedback loops, core *clock* gene expressions generate an endogenous rhythm of numerous protein expressions, leading to rhythmic functioning of cells and tissues that oscillates over an approximately 24-hour period (Dunlap, 2006). The molecular clock has been demonstrated to modulate energy metabolism by controlling the expression and activity of numerous enzymes, transport systems and nuclear receptors involved in lipid and carbohydrate metabolism (Ramsey et al., 2007); (Staels, 2006); (Yang et al., 2006).

Recent studies have suggested that, in murine models, malfunctioning of molecular clock genes, such as *Bmal1* (Rudic et al., 2004) and *Clock* (Turek et al., 2005), is involved in development of the metabolic syndrome. In addition, in humans, prevalences of obesity, T2DM and features of the metabolic syndrome are reportedly increased in nightshift workers and men with short sleep durations (Prasai et al., 2008). Thus, the importance of the molecular clock for many metabolic processes has been extensively documented. On the other hand, to our knowledge, there have been no studies showing that obesity itself attenuates rhythmic expressions of clock genes in the CNS. Rather, a high fat diet does not affect rhythmic expression profiles of core clock genes, such as *Bmal1* and *Per2*, in the mediobasal hypothalamus, whereas it does attenuate circadian expression of these core clock genes in the liver and adipose tissue (Kohsaka et al., 2007). In genetically obese and diabetic mice as well, circadian expression of neither *Per1* nor *Per2* is altered in the suprachiasmatic nucleus (SCN), while both are attenuated in the liver (Kudo et al., 2004). Based on these findings, the idea that obesity affects molecular clock function in peripheral tissues but not centrally has been proposed (Prasai et al., 2008). However, metabolic alterations disturb the patterns and/or circadian rhythmicity of behaviors, such as sleep-wake cycle (Danguir, 1989); (Jenkins et al., 2006); (Laposky et al., 2006); (Megirian et al., 1998), locomotor activity and feeding (Kohsaka et al., 2007), indicating rhythmic perturbation in the CNS. Therefore, in the present study, we examined whether obesity per se alters circadian expressions of clock genes in the CNS, especially in the caudal brainstem nucleus of the solitary tract (NTS).

Recently, we have demonstrated that alterations in fat accumulation in intra-abdominal organs, such as visceral adipose tissue and the liver, send afferent neuronal signals to the brain, leading to modulation of feeding behavior as well as efferent sympathetic tonus (Uno et al., 2006); (Yamada et al., 2006). These neuronal signals are likely to initially be processed mainly by the NTS (Grill, 2006); (Schwartz, 2006), since the NTS receives neuronal projections of vagal and non-vagal afferents (Menetrey and Basbaum, 1987); (Menetrey and De Pommery, 1991). In addition, humoral factors, such as leptin, insulin and glucose, may directly impinge on neuronal activities in the NTS (Grill, 2006); (Schwartz, 2006). Furthermore, the NTS and the hypothalamic nuclei send neuronal projections to each other. Thus, we postulate that the NTS is ideally situated for integrating central and peripheral metabolic signals. Therefore, we focused on the circadian expressions of clock genes in the NTS.

2. Results

2.1. *Rhythmic mRNA expressions of clock genes in the NTS of C57BL/6 mice*

To investigate whether the mRNA expressions of clock genes show circadian rhythms in the NTS, we first analyzed wild-type lean control mice, 10-week-old C57BL/6 mice fed a regular chow diet (CD mice). Bilateral NTS samples at the level of the area postrema were obtained every 4 h throughout a single 24-h period employing a laser micro-dissection procedure (Fig.1A). *Clock* and *Cry1* expressions did not show circadian rhythms in the NTS (Fig. 1B). In contrast, other clock genes we examined (*Npas2* (a *Clock* homolog), *Bmal1*, *Per1*, *Per2* and *Rev-erbα*) all exhibited 24-h rhythmicity. The transcript levels of *Bmal1* and *Npas2* peaked in the first half of the light phase. On the other hand, the *Per1* and *Per2* mRNA simultaneously dropped to near trough levels (Fig. 1B). The NPAS2/BMAL1 complex reportedly induces transcription of *Per* genes (Reick et al., 2001). In addition, the rhythmicity of these clock genes was also observed in the NTS of 15-week-old C57BL/6 mice and no significant differences in the expression profiles of these clock genes were detected between 10-and 15-week-old C57BL/6 mice (Fig. 1C). These results indicate that an intracellular circadian clock system actually operates in the NTS.

2.2. *Alterations in circadian mRNA expression profiles of clock genes in the NTS of obesity models*

Next, we examined whether obesity affects the circadian expressions of clock genes in the NTS. As shown in Fig. 2, C57BL/6 mice fed a high fat diet for 10 weeks (HFD mice), KK-A^y and *ob/ob* (leptin-deficient) mice were significantly heavier than CD mice. Serum insulin levels were significantly increased in all these murine obesity models. In addition, blood glucose levels were markedly increased in KK-A^y and *ob/ob* mice. Serum leptin levels were also increased in HFD and KK-A^y mice. Serum free fatty acid levels were markedly increased in KK-A^y and *ob/ob* mice but

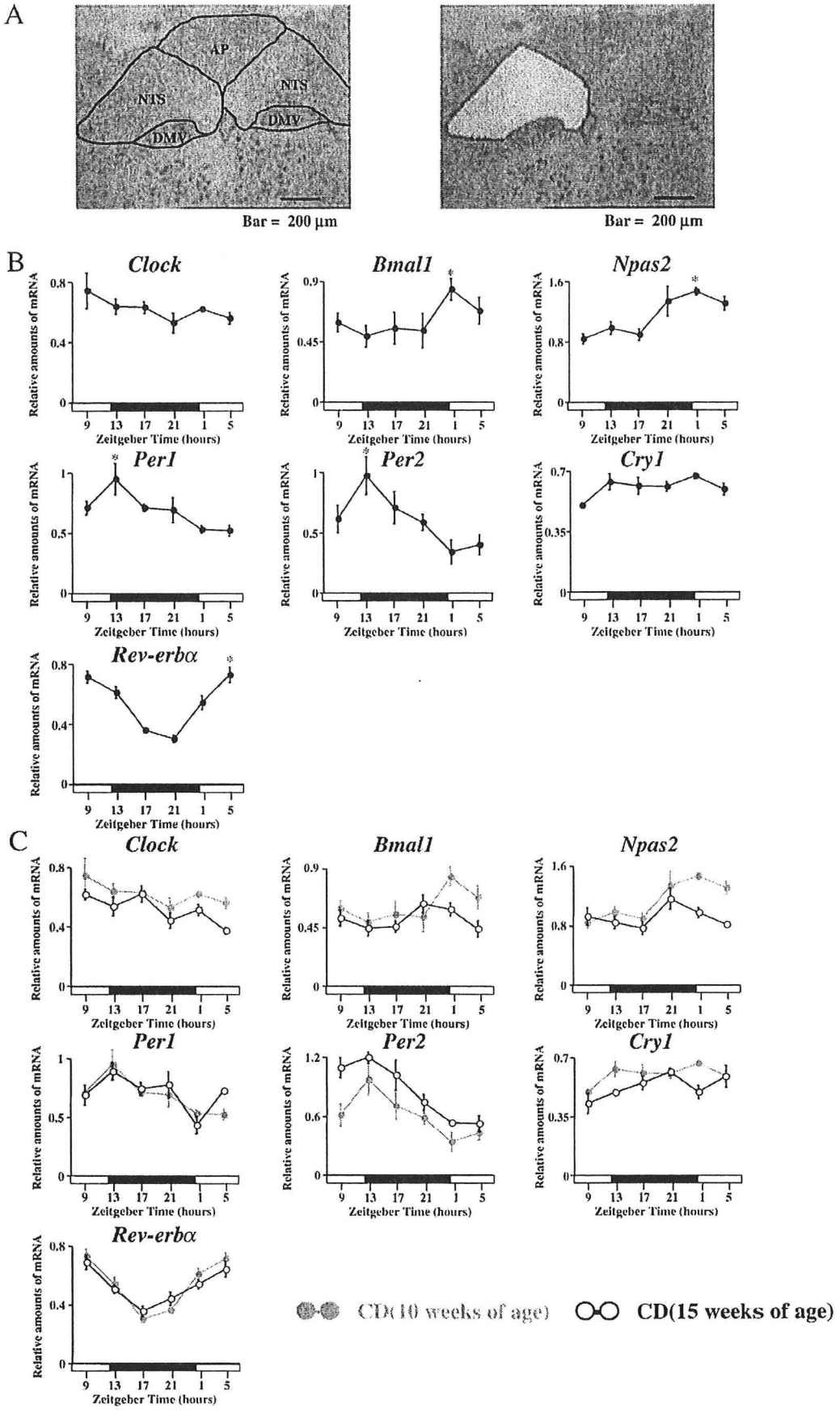
A
AP
NTS
NTS
DMV
DMV
Bar = 200 μm
Bar = 200 μm
B
Clock
Bmal1
Npas2
Per1
Per2
Cry1
Rev-erbα
Relative amounts of mRNA
Zeitgeber Time (hours)
C
Clock
Bmal1
Npas2
Per1
Per2
Cry1
Rev-erbα
CD(10 weeks of age)
CD(15 weeks of age)

not in HFD mice (Fig. 2). These findings suggest that severe insulin resistance is induced in KK-A^y and *ob/ob* mice, while that in HFD mice is milder.

To examine the hypothesis that obesity affects expressions of clock genes, we analyzed the circadian expressions of transcripts encoding CLOCK, NPAS2, BMAL1, PER1, PER2, CRY1 and REV-ERBα in the NTS of these murine obesity models. The rhythms and levels of expressions of these clock genes in the NTS of murine obesity models were compared with those in age-matched CD mice (HFD mice vs 15-week-old CD mice and KK-A^y and *ob/ob* mice vs 10-week-old CD mice). As shown in Fig. 3, the levels of *Clock* expression were significantly increased at several observation times in HFD mice. Interestingly, rhythms of *Bmal1* expression in the NTS were significantly altered in HFD (2-way ANOVA; $F=11.54$, $P=2.0\times10^{-7}$) and KK-A^y (2-way ANOVA; $F=4.01$, $P=4.9\times10^{-3}$) mice and levels were significantly increased in HFD, KK-A^y and *ob/ob* mice. The *Per2* expression level tended to be increased in KK-A^y mice, although the difference did not reach statistical significance. The *Cry1* expression level was significantly decreased in KK-A^y and *ob/ob* mice. Furthermore, in addition to decreased expression levels of *Rev-erbα*, the rhythms of its expression were significantly altered in the NTS of HFD (2-way ANOVA; $F=2.49$, $P=4.6\times10^{-2}$), KK-A^y (2-way ANOVA; $F=12.02$, $P=3.0\times10^{-7}$) and *ob/ob* mice (2-way ANOVA; $F=7.90$, $P=2.8\times10^{-5}$) (Fig. 3). Collectively, these findings suggest that obesity with insulin resistance alters profiles of rhythmic clock gene expressions in the NTS and generates gene-specific changes in circadian expression patterns.

2.3. *The mRNA expression profiles of clock-related genes in the NTS of obesity models*

What mechanisms alter the expression profiles of clock genes? Transcriptional activity of peroxisome proliferator-activated receptor α (PPARα), a member of the nuclear receptor superfamily, is up-regulated in the livers of mice with obesity and diabetes (Memon et al., 2000). In addition, the CLOCK/BMAL1 heterodimer activates the transcription of PPARα, which then binds to the peroxisome proliferator response element and thereby induces *Bmal1* transcription in the liver (Canaple et al., 2006). In addition, PPARα is reportedly expressed in the NTS, but not in the hypothalamus (Moreno et al., 2004). These findings prompted us to theorize that PPARα affects the mRNA expression profiles of clock genes. Therefore, we analyzed mRNA expression profiles of PPARα in the NTS of CD mice as well as that of murine models of obesity and insulin resistance. In both CD and obese mice (HFD, KK-A^y and *ob/ob* mice), PPARα expression in the NTS showed no 24-h rhythmicity (Fig. 4A). However, the mRNA expression level of PPARα was significantly increased in the NTS of HFD and KK-A^y mice. In addition, in the NTS of *ob/ob* mice, the PPARα expression level tended to be increased and *carnitine palmitoyltransferase-1α* (CPT1α), a downstream target of PPARα, was significantly up-regulated, suggesting functional activation of PPARα (Fig. 4A). Thus, PPARα in the NTS might be involved in the altered expression profiles of clock genes.

Next, to investigate whether alterations in circadian expressions of clock genes affect neuronal function in the NTS, we analyzed the mRNA expression levels of downstream targets of clock genes, *Kcnma1* and *tyrosine hydroxylase* (*TH*), both of which are involved in neuronal activity. Daily expression of *Kcnma1*, the large conductance Ca^{2+}-activated K^+(BK) channel, is reportedly controlled by the intrinsic circadian clock in the SCN (Meredith et al., 2006); (Panda et al., 2002). The circadian expression profile of *TH*, the rate-limiting enzyme in catecholamine synthesis, is also affected by *Clock* in the midbrain ventral tegmental area (McClung et al., 2005). As reportedly observed in the SCN (Panda et al., 2002), *Kcnma1* in the NTS of CD mice was highly expressed in the early portion of the dark phase (Fig. 4B). In contrast, this *Kcnma1* expression pattern disappeared and expression levels were markedly decreased in the NTS of all three murine obesity models (Fig. 4B). In addition, *TH* expression levels in *ob/ob* mice were significantly decreased as compared to those in CD mice (Fig. 4B). Collectively, obesity-induced alterations in expression profiles of clock-related genes, such as *Kcnma1* and *TH*, might elicit neuronal dysfunctions in the NTS, although further studies are needed to confirm this possibility.

3. Discussion

In the present study, we demonstrated the circadian expressions of a series of core clock genes in the NTS of lean wild-type mice. In addition, the circadian expressions of core clock genes and their downstream targets were shown to be attenuated in the NTS of obesity models, suggesting the involvement of NTS rhythmic perturbation in further metabolic deterioration in the obese state.

Metabolism is coordinated and regulated among different organs/tissues throughout the body. This coordinated metabolic regulation is apparently essential for maintaining systemic homeostasis, particularly energy metabolism. Metabolic communication among organs/tissues and integration of metabolic information in various tissues thus appears to be important and perturbation of this control system may lead to the development of metabolic disorders (Katagiri et al., 2007). This controlling system is likely to consist of afferent and efferent limbs as well as a central control mechanism putatively situated in the CNS (Yamada et al., 2008). For the afferent limb, there are two avenues, humoral factors and

Fig. 1 – Rhythmic mRNA expressions of clock genes in the NTS of C57BL/6 mice. (A) Coronal section of mouse brainstem within the NTS region of before laser micro-dissection (left). The NTS removed at the area postrema level (right). AP, area postrema; DMV, dorsal motor nucleus of the vagus. (B) Daily mRNA expression profiles of *clock* genes in the NTS of 10-week-old C57BL/6 mice, which had been maintained under a 12-h light, 12-h dark cycle and fed a standard diet. (C) Daily mRNA expression profiles of *clock* genes in the NTS of 15-week-old C57BL/6 mice (○-○), which had been maintained under a 12-h light, 12-h dark cycle and fed a standard diet. Data are presented as means ± SE ($n=4$–5/group). 1-way ANOVA demonstrates significant rhythmicity of *Npas2*, *Bmal1*, *Per1*, *Per2* and *Rev-erbα* mRNA levels ($P<0.05$). *Indicates peaks of rhythmically expressed each mRNA.

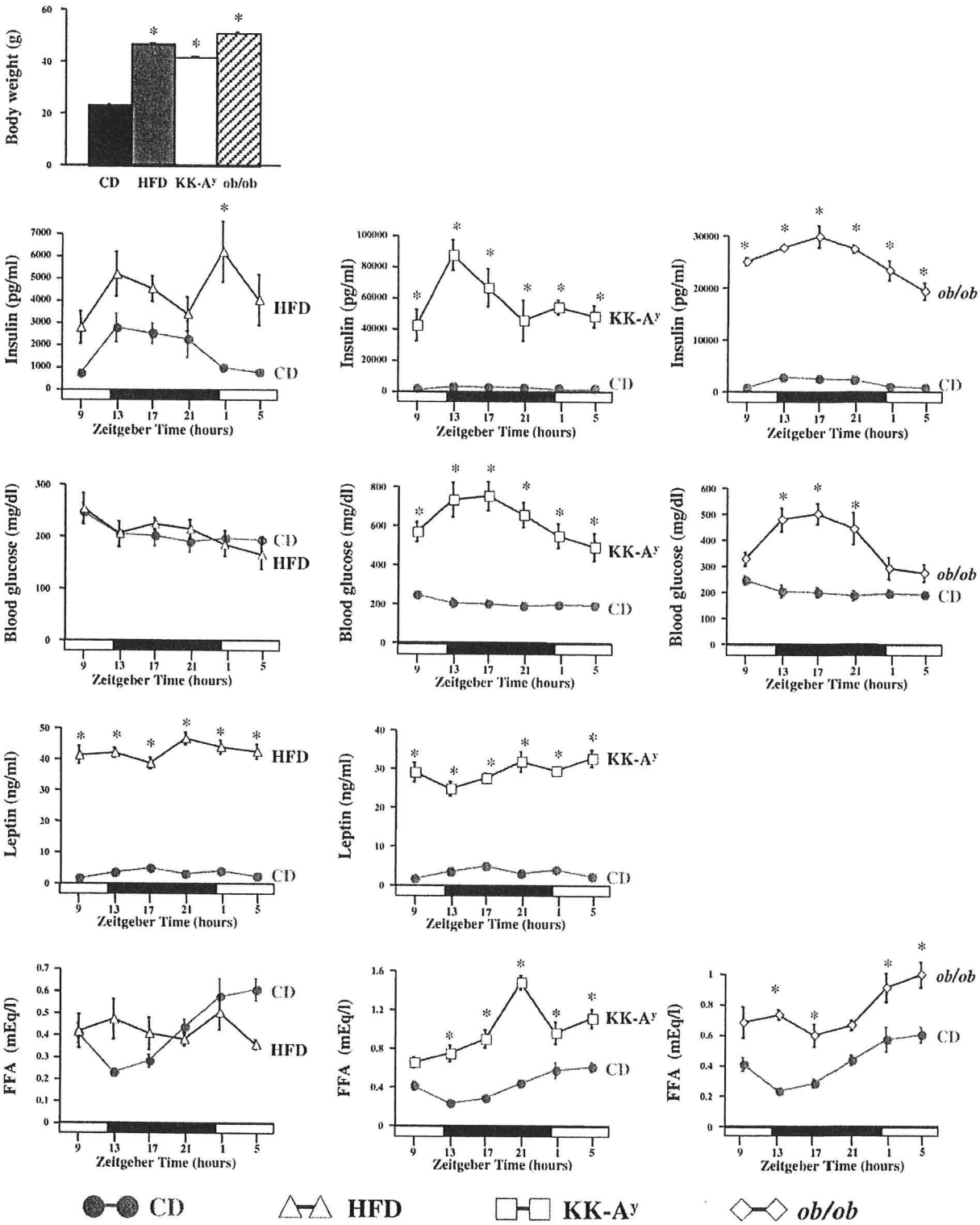

Fig. 2 – Metabolic parameters of murine obesity models. Body weight and diurnal variations in blood glucose, serum insulin, leptin and free fatty acid (FFA) levels of CD mice (●–●), HFD mice (△–△), KK-A^y mice (□–□) and *ob/ob* mice (◇–◇). Data are presented as means ± SE (n=4–5/group). Body weights were analyzed by 1-way ANOVA. The statistical significance of differences between two groups was determined using 2-way ANOVA followed by Tukey's post hoc test. *Indicates $P<0.05$.

afferent neuronal signals. For instance, mechanical, nutrient chemical and gut peptide signals are sent from the gastrointestinal tract by primary afferent neurons of the vagus and from the dorsal root (Badman and Flier, 2005). In addition, we have recently demonstrated that information regarding lipid metabolism in intra-abdominal tissues, such as visceral adipose tissue and the liver, is conveyed to the brain via afferent nerves, leading to modulation of feeding behavior and sympathetic tonus (Uno et al., 2006); (Yamada et al., 2006). These neuronal signals are initially processed mainly by the NTS (Grill, 2006); (Schwartz, 2006). In addition, receptors for humoral factors, such as leptin and insulin, are reportedly expressed on NTS neurons (Grill, 2006); (Schwartz, 2006). Furthermore, the NTS sends projections to other autonomic nuclei at all levels of the neuroaxis, including major targets in the hypothalamus, pons and medulla (Hermes et al., 2006). NTS neurons in turn receive descending projections from a variety of hypothalamic nuclei implicated in the control of energy homeostasis (Grill, 2006); (Schwartz, 2006). Thus, the NTS seems to be ideally situated to integrate central and peripheral signals. In the present study, the circadian expressions of a series of core clock genes, including *Npas2*, *Bmal1*, *Per1*, *Per2* and *Rev-erbα*, were demonstrated in the NTS of lean wild-type mice, results consistent with those of a previous report describing rhythmic expressions of *Bmal1* and *Per2* in the rat NTS (Herichova et al., 2007).

Recent studies have suggested that rhythmic abnormalities affect energy homeostasis as well as glucose and lipid metabolism (Prasai et al., 2008); (Rudic et al., 2004); (Turek et al., 2005). Metabolic perturbation, in turn, reportedly induces dysregulation of circadian rhythms in the periphery. In fact, both genetically induced and high fat diet-induced obesity attenuates the circadian expressions of a number of clock genes in peripheral tissues, such as adipose and the liver (Ando et al., 2006); (Ando et al., 2005); (Kohsaka et al., 2007); (Kudo et al., 2004). In addition, metabolic alterations disturb patterns and/or the circadian rhythmicity of behaviors, such as the sleep-wake cycle, locomotor activity and feeding. For example, mice fed a high-fat diet have longer sleep times but less sleep consolidation (Jenkins et al., 2006). Genetic mouse (Laposky et al., 2006) and rat (Danguir, 1989); (Megirian et al., 1998) models of obesity exhibit disrupted sleep-wake patterns. High-fat diet also leads to changes in the period of locomotor activity and feeding rhythm in mice (Kohsaka et al., 2007). Since these behavioral abnormalities indicate CNS dysfunction, these findings suggest circadian malfunction in the CNS. However, obesity reportedly has no effects molecular clock genes in the hypothalamus (Kohsaka et al., 2007) and the SCN (Kudo et al., 2004). In the present study, we showed both high fat diet-induced and genetically induced obesity to affect circadian expression profiles of core clock genes, such as *Clock*, *Bmal1*, *Rev-erbα* and *Cry1* in the NTS. This is the first report to demonstrate that circadian expression profiles of clock genes in the CNS are perturbed by obesity.

A major question arising from these findings involves the nature of the molecular link between the regulation of metabolism and the circadian rhythmicity of clock genes. We showed that both PPARα transcription and the *Bmal1* expression level were increased in the NTS of obese mice. Obesity reportedly enhances PPARα transcriptional activity in the liver (Memon et al., 2000). PPARα binds to the PPRE and induces transcription of *Bmal1* (Canaple et al., 2006). In addition, amplitudes of *Bmal1* expression are reportedly decreased in the livers of PPARα knockout mice (Canaple et al., 2006), which is in line with the findings of this study. Therefore, PPARα might be directly involved in obesity-induced enhancement of *Bmal1* expression in the NTS, although further studies are needed to confirm this conclusion. Furthermore, we found that *Rev-erbα* expression was decreased in the NTS of obese mice. *Rev-erbα* transcription is inhibited by retinoic acid (Chawla and Lazar, 1993), levels of which are increased in the metabolic syndrome (Yang et al., 2005). These findings prompt us to hypothesize that high concentrations of retinoic acid would decrease expression levels of *Rev-erbα* in the NTS of mice with obesity and insulin resistance. In addition, because *Bmal1* transcription is inhibited by REV-ERBα (Chawla and Lazar, 1993); (Preitner et al., 2002), decreased *Rev-erbα* expression may in turn contribute to increased *Bmal1* expression.

Finally, we showed that the expression profiles of downstream targets of clock genes were affected by obesity associated with insulin resistance. The expression profile of *Kcnma1*, a downstream target of clock genes (Meredith et al., 2006); (Panda et al., 2002), was attenuated in the NTS of obese mice. Since the BK channel is believed to play a critical role in the control of neurosecretion (Lara et al., 1999); (Lovell and McCobb, 2001), attenuated expression of *Kcnma1* might underlie the neuronal dysfunction in obese states. In addition, *TH* mRNA expression was decreased in the NTS of *ob/ob* mice. Recent reports have demonstrated that neural pathways from catecholamine neurons in the NTS to the hypothalamus are involved in energy homeostasis (Date et al., 2006); (Ritter et al., 2003). Therefore, these findings suggest that perturbation of circadian expression profiles of clock genes in the NTS is involved in further metabolic deterioration of energy homeostasis.

In summary, this study showed that a series of core clock genes exhibit circadian rhythms in the NTS of the brainstem. However, these rhythmic expressions are perturbed in murine models with high fat diet-induced or genetically induced obesity and insulin resistance. Obesity also alters expressions of *PPARα* and downstream targets of clock genes, which might account for the mechanisms underlying the rhythmic disruption and neuronal dysfunction in obese states. This is the first report showing that obesity perturbs the circadian expressions of core clock genes in the CNS.

4. Experimental procedures

4.1. *Animals*

Male C57BL/6 mice (Kyudo, Kumamoto, Japan), KK-A^y mice (CLEA Japan, Tokyo, Japan) and *ob/ob* mice (strain C57BL/6 *ob/ob*) (Charles River Japan, Yokohama, Japan) were obtained and maintained under specific-pathogen free conditions with controlled temperature and humidity and a 12-h light (0600–1800), 12-h dark (1800–0600) cycle. According to the breeder

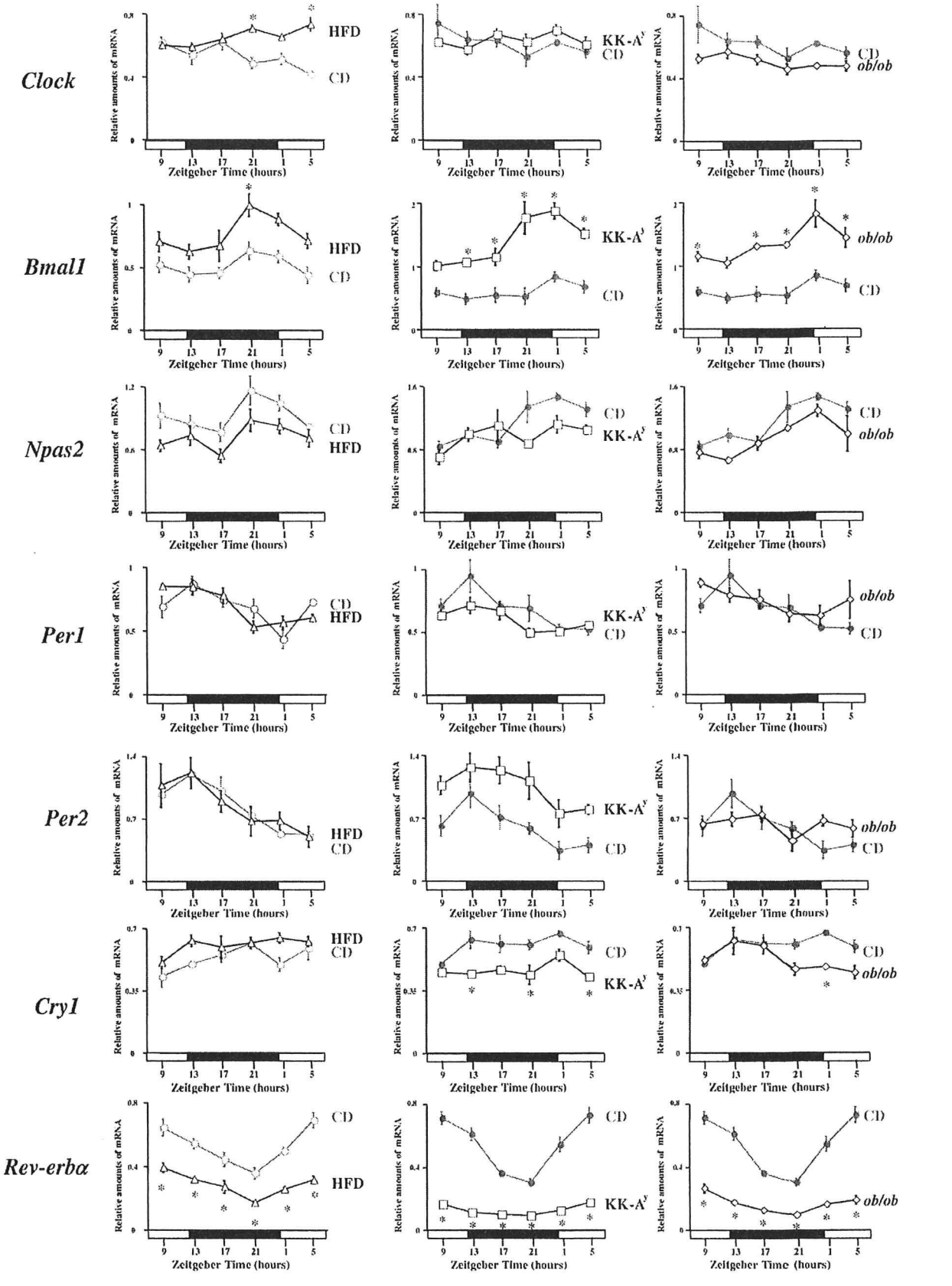
Clock
Bmal1
Npas2
Per1
Per2
Cry1
Rev-erbα
HFD
CD
KK-Ay
ob/ob
Relative amounts of mRNA
Zeitgeber Time (hours)
CD(10 weeks of age)
CD(15 weeks of age)
HFD
KK-Ay
ob/ob

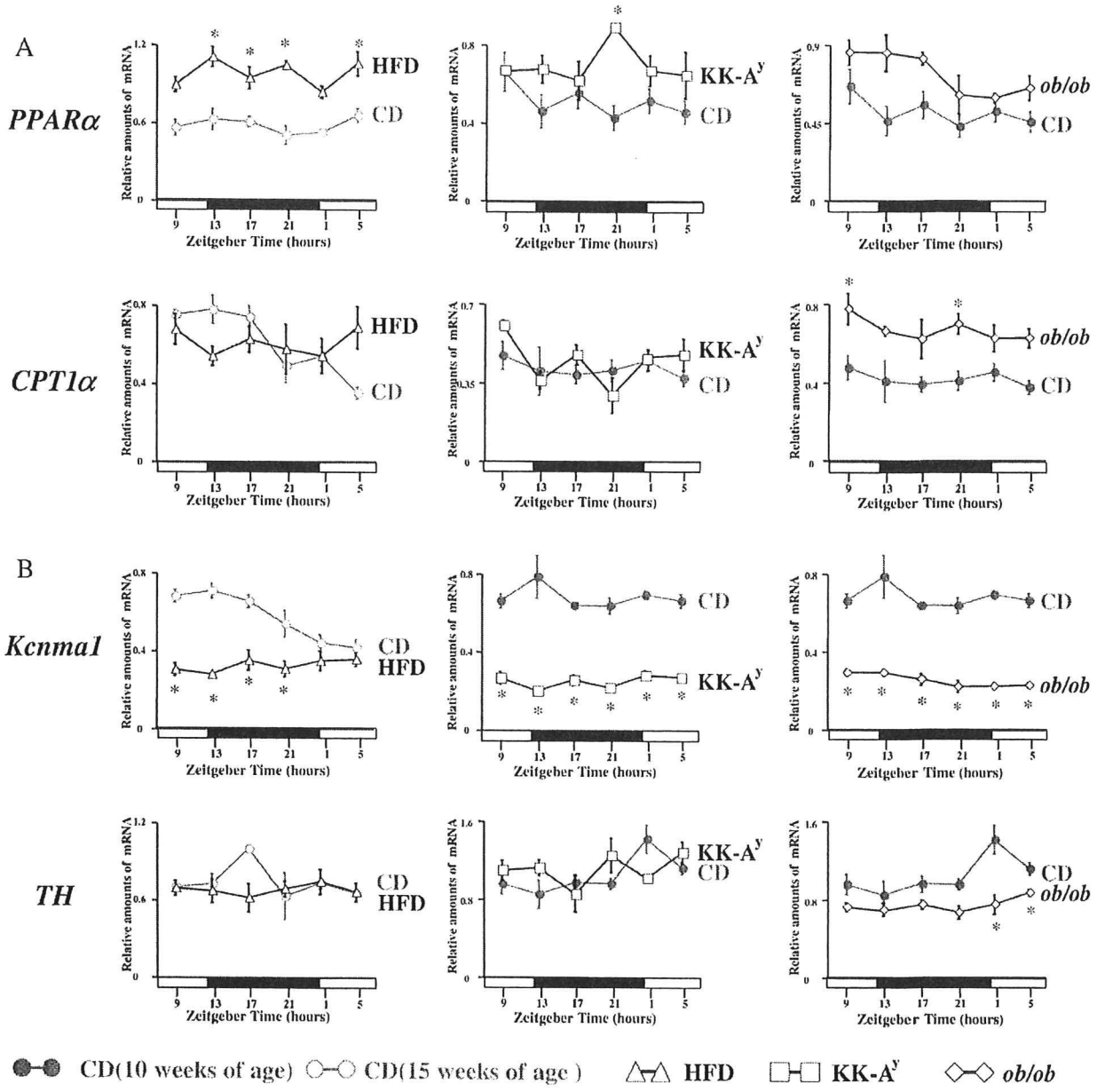

Fig. 4 – mRNA expression profiles of clock-related genes in NTS of obesity models. Daily mRNA expression profiles of PPARα and CPT1α (A), *Kcnma1* and *TH* (B) in the NTS of 10-week-old CD mice (●–●), 15-week-old CD mice (○–○), HFD mice (△–△), KK-A^y mice (□–□) and *ob/ob* mice (◇–◇). Data are presented as means ± SE (n = 4–5/group). *$P < 0.05$ by 2-way ANOVA followed by Tukey's post hoc test.

(CLEA Japan, Tokyo, Japan) information, KK-A^y mice were generated by crossing KK mice with C57BL/6-A^y mice. KK mice are mildly obese and insulin resistant (Ando et al., 2006); (Yamada et al., 2006). Therefore, as reported previously (Ando et al., 2006), to examine whether obesity per se alters circadian expressions of clock genes in the CNS, we used C57BL/6 mice, rather than KK mice, as lean controls for KK-A^y mice. Mice were housed individually and given a standard laboratory diet (65% carbohydrate, 4% fat, 24% protein) and water *ad libitum*. These animals, at 10 weeks of age, were sacrificed to obtain blood and brain samples at the following zeitgeber times (ZTs): 1, 5, 9, 13, 17 and 21, in which ZT 0 is defined as lights on and

Fig. 3 – Alterations in circadian mRNA expression profiles of *clock* genes in NTS of obesity models Daily mRNA expression profiles of *clock* genes in the NTS of 10-week-old CD mice (●–●), 15-week-old CD mice (○–○), HFD mice (△–△), KK-A^y mice (□–□) and *ob/ob* mice (◇–◇). Data are presented as means ± SE (n = 4–5/group). *$P < 0.05$ by 2-way ANOVA followed by Tukey's post hoc test.

Table 1 – Sequences of quantitative RT-PCR primers

Gene	Primer 1	Primer 2
Clock	5′-agatcagttcaatgtcctca-3′	5′-tgtcgaatctcactagcatc-3′
Bmal1	5′-cgtcgggacaaaatgaaca-3′	5′-ttctgtgtatgggttggtgg-3′
Npas2	5′-cagcagccaccaccctatt-3′	5′-tgcggaggtgtagactgtgt-3′
Per1	5′-gtactttggcagcatcgactc-3′	5′-cggtcttgcttcagcacaga-3′
Per2	5′-cagccaccctgaaaagga-3′	5′-gtgagggacaccacactctc-3′
Cry1	5′-cggtggaaattgctctca-3′	5′-ggcatcctcttcctgacta-3′
Rev-erbα	5′-aactccctggcacttacc-3′	5′-gttcttcagcaccagagc-3′
PPARα	5′-tccctgtttgtggctgctat-3′	5′-ttgggaagaggaaggtgtca-3′
CPT1α	5′-gagccatgaagccctcaaacagat-3′	5′-gctgtacaacatgggctttcgacc-3′
Kcnma1	5′-ggatggtggttgttatggtg-3′	5′-tcgtagggaggattggtgat-3′
TH	5′-ggctgctgtcttcctatggaga-3′	5′-atgggcgctggatacgaga-3′
GAPDH	5′-tgaaggtcggtgtgaacg-3′	5′-ccattctcggccttgact-3′

PPARα, *peroxisome proliferator-activated receptor α*
CPT1α, *carnitine palmitoyl-transferase-1α*
TH, tyrosine hydroxylase
GAPDH, *glyceraldehyde-3-phosphate dehydrogenase*

ZT 12 as light off. High-fat-chow feeding (32% safflower oil, 33.1% casein, 17.6% sucrose, and 5.6% cellulose) (Yamada et al., 2006) was initiated at 5 weeks of age in C57BL/6 mice and continued for 10 weeks. All animal studies were conducted in accordance with the institutional guidelines for animal experiments at Tohoku University.

4.2. *Blood analysis*

Blood glucose and serum insulin, leptin, and free fatty acid levels were determined as previously described (Yamada et al., 2006).

4.3. *Tissue preparation*

All animals were sacrificed by decapitation at the indicated ZTs. The brains were immediately frozen in isopentane on dry ice and stored at-80 °C until RNA purification.

4.4. *Laser micro-dissection*

Coronal cryostat sections (20 μm) through the bilateral NTS at the level of the area postrema (Fig. 1A) were placed on PEN-coated slides (Leica Microsystems). Laser micro-dissection was carried out on a Leica AS LMD (Leica Microsystems). Immediately after micro-dissection, the samples were placed on dry ice and then stored at a-80 °C until RNA purification.

4.5. *RNA purification and quantitative real-time PCR (qRT-PCR)*

Total RNA was purified from 10 20-micron laser micro-dissected NTS specimens with an RNeasy microkit (QIAGEN, Valencia, CA, USA), and cDNA synthesized from total RNA was evaluated with a real-time PCR quantitative system (Light Cycler Quick System 350S; Roche Diagnostics GmbH, Mannheim, Germany) as previously reported (Yamada et al., 2006).The relative amount of mRNA was calculated with GAPDH mRNA as the invariant control. The primers used are shown in Table 1.

4.6. *Statistics*

The results are presented as means ± SE. Body weights and time-series data were analyzed by 1-way ANOVA to determine significant differences. The statistical significance of differences between two groups was determined using 2-way ANOVA followed by Tukey's post hoc test.

Acknowledgments

We thank Ms. I. Sato, J. Fushimi, K. Aizawa and T. Takasugi for technical support. This work was supported by Grants-in-Aid for Scientific Research (B2, 15390282) to H.K. from the Japanese Ministry of Education, Science, Sports and Culture, and a Grant-in-Aid for Scientific Research (H19-genome-005) to Y.O. from the Japanese Ministry of Health, Labor and Welfare. This work was also supported by the Global-COE Program to Y.O. and the 21st Century COE Program to H.K. from the Japanese Ministry of Education, Science, Sports and Culture.

REFERENCES

Ando, H., Yanagihara, H., Hayashi, Y., Obi, Y., Tsuruoka, S., Takamura, T., Kaneko, S., Fujimura, A., 2005. Rhythmic messenger ribonucleic acid expression of clock genes and adipocytokines in mouse visceral adipose tissue. Endocrinology 146, 5631–5636.

Ando, H., Oshima, Y., Yanagihara, H., Hayashi, Y., Takamura, T., Kaneko, S., Fujimura, A., 2006. Profile of rhythmic gene expression in the livers of obese diabetic KK-A(y) mice. Biochem. Biophys. Res. Commun. 346, 1297–1302.

Badman, M.K., Flier, J.S., 2005. The gut and energy balance: visceral allies in the obesity wars. Science 307, 1909–1914.

Canaple, L., Rambaud, J., Dkhissi-Benyahya, O., Rayet, B., Tan, N.S., Michalik, L., Delaunay, F., Wahli, W., Laudet, V., 2006.

Reciprocal regulation of brain and muscle Arnt-like protein 1 and peroxisome proliferator-activated receptor alpha defines a novel positive feedback loop in the rodent liver circadian clock. Mol. Endocrinol. 20, 1715–1727.
Chawla, A., Lazar, M.A., 1993. Induction of Rev-ErbA alpha, an orphan receptor encoded on the opposite strand of the alpha-thyroid hormone receptor gene, during adipocyte differentiation. J. Biol. Chem. 268, 16265–16269.
Danguir, J., 1989. Sleep patterns in the genetically obese Zucker rat: effect of acarbose treatment. Am. J. Physiol. 256, R281–283.
Date, Y., Shimbara, T., Koda, S., Toshinai, K., Ida, T., Murakami, N., Miyazato, M., Kokame, K., Ishizuka, Y., Ishida, Y., Kageyama, H., Shioda, S., Kangawa, K., Nakazato, M., 2006. Peripheral ghrelin transmits orexigenic signals through the noradrenergic pathway from the hindbrain to the hypothalamus. Cell. Metab. 4, 323–331.
Dunlap, J.C., 2006. Physiology. Running a clock requires quality time together. Science 311, 184–186.
Flier, J.S., 2004. Obesity wars: molecular progress confronts an expanding epidemic. Cell 116, 337–350.
Grill, H.J., 2006. Distributed neural control of energy balance: contributions from hindbrain and hypothalamus. Obesity (Silver Spring) 14 (Suppl. 5), 216S–221S.
Herichova, I., Mravec, B., Stebelova, K., Krizanova, O., Jurkovicova, D., Kvetnansky, R., Zeman, M., 2007. Rhythmic *clock* gene expression in heart, kidney and some brain nuclei involved in blood pressure control in hypertensive TGR(mREN-2)27 rats. Mol. Cell. Biochem. 296, 25–34.
Hermes, S.M., Mitchell, J.L., Aicher, S.A., 2006. Most neurons in the nucleus tractus solitarii do not send collateral projections to multiple autonomic targets in the rat brain. Exp. Neurol. 198, 539–551.
Jenkins, J.B., Omori, T., Guan, Z., Vgontzas, A.N., Bixler, E.O., Fang, J., 2006. Sleep is increased in mice with obesity induced by high-fat food. Physiol. Behav. 87, 255–262.
Katagiri, H., Yamada, T., Oka, Y., 2007. Adiposity and cardiovascular disorders: disturbance of the regulatory system consisting of humoral and neuronal signals. Circ. Res. 101, 27–39.
Kohsaka, A., Laposky, A.D., Ramsey, K.M., Estrada, C., Joshu, C., Kobayashi, Y., Turek, F.W., Bass, J., 2007. High-fat diet disrupts behavioral and molecular circadian rhythms in mice. Cell. Metab. 6, 414–421.
Kudo, T., Akiyama, M., Kuriyama, K., Sudo, M., Moriya, T., Shibata, S., 2004. Night-time restricted feeding normalises clock genes and *Pai*-1 gene expression in the db/db mouse liver Diabetologia 47, 1425–1436.
Laposky, A.D., Shelton, J., Bass, J., Dugovic, C., Perrino, N., Turek, F. W., 2006. Altered sleep regulation in leptin-deficient mice. Am. J. Physiol., Regul. Integr. Comp. Physiol. 290, R894–903.
Lara, J., Acevedo, J.J., Onetti, C.G., 1999. Large-conductance Ca2+-activated potassium channels in secretory neurons. J. Neurophysiol. 82, 1317–1325.
Lovell, P.V., McCobb, D.P., 2001. Pituitary control of BK potassium channel function and intrinsic firing properties of adrenal chromaffin cells. J. Neurosci. 21, 3429–3442.
McClung, C.A., Sidiropoulou, K., Vitaterna, M., Takahashi, J.S., White, F.J., Cooper, D.C., Nestler, E.J., 2005. Regulation of dopaminergic transmission and cocaine reward by the *Clock* gene. Proc. Natl. Acad. Sci. U. S. A. 102, 9377–9381.
Megirian, D., Dmochowski, J., Farkas, G.A., 1998. Mechanism controlling sleep organization of the obese Zucker rats. J. Appl. Physiol. 84, 253–256.
Memon, R.A., Tecott, L.H., Nonogaki, K., Beigneux, A., Moser, A.H., Grunfeld, C., Feingold, K.R., 2000. Up-regulation of peroxisome proliferator-activated receptors (PPAR-alpha) and PPAR-gamma messenger ribonucleic acid expression in the liver in murine obesity: troglitazone induces expression of PPAR-gamma-responsive adipose tissue-specific genes in the liver of obese diabetic mice. Endocrinology 141, 4021–4031.
Menetrey, D., Basbaum, A.I., 1987. Spinal and trigeminal projections to the nucleus of the solitary tract: a possible substrate for somatovisceral and viscerovisceral reflex activation. J. Comp. Neurol. 255, 439–450.
Menetrey, D., De Pommery, J., 1991. Origins of spinal ascending pathways that reach central areas involved in visceroception and visceronociception in the rat. Eur. J. Neurosci. 3, 249–259.
Meredith, A.L., Wiler, S.W., Miller, B.H., Takahashi, J.S., Fodor, A.A., Ruby, N.F., Aldrich, R.W., 2006. BK calcium-activated potassium channels regulate circadian behavioral rhythms and pacemaker output. Nat. Neurosci. 9, 1041–1049.
Moreno, S., Farioli-Vecchioli, S., Ceru, M.P., 2004. Immunolocalization of peroxisome proliferator-activated receptors and retinoid X receptors in the adult rat CNS. Neuroscience 123, 131–145.
Panda, S., Antoch, M.P., Miller, B.H., Su, A.I., Schook, A.B., Straume, M., Schultz, P.G., Kay, S.A., Takahashi, J.S., Hogenesch, J.B., 2002. Coordinated transcription of key pathways in the mouse by the circadian clock. Cell 109, 307–320.
Prasai, M.J., George, J.T., Scott, E.M., 2008. Molecular clocks, type 2 diabetes and cardiovascular disease. Diab. Vasc. Dis. Res. 5, 89–95.
Preitner, N., Damiola, F., Lopez-Molina, L., Zakany, J., Duboule, D., Albrecht, U., Schibler, U., 2002. The orphan nuclear receptor REV-ERBalpha controls circadian transcription within the positive limb of the mammalian circadian oscillator. Cell 110, 251–260.
Ramsey, K.M., Marcheva, B., Kohsaka, A., Bass, J., 2007. The clockwork of metabolism. Annu. Rev. Nutr. 27, 219–240.
Reick, M., Garcia, J.A., Dudley, C., McKnight, S.L., 2001. NPAS2: an analog of clock operative in the mammalian forebrain. Science 293, 506–509.
Ritter, S., Watts, A.G., Dinh, T.T., Sanchez-Watts, G., Pedrow, C., 2003. Immunotoxin lesion of hypothalamically projecting norepinephrine and epinephrine neurons differentially affects circadian and stressor-stimulated corticosterone secretion. Endocrinology 144, 1357–1367.
Rudic, R.D., McNamara, P., Curtis, A.M., Boston, R.C., Panda, S., Hogenesch, J.B., Fitzgerald, G.A., 2004. BMAL1 and CLOCK, two essential components of the circadian clock, are involved in glucose homeostasis. PLoS Biol. 2, e377.
Sandoval, D., Cota, D., Seeley, R.J., 2008. The integrative role of CNS fuel-sensing mechanisms in energy balance and glucose regulation. Annu. Rev. Physiol. 70, 513–535.
Schibler, U., Sassone-Corsi, P., 2002. A web of circadian pacemakers. Cell 111, 919–922.
Schwartz, G.J., 2006. Integrative capacity of the caudal brainstem in the control of food intake. Philos. Trans. R. Soc. Lond., B Biol. Sci. 361, 1275–1280.
Staels, B., 2006. When the clock stops ticking, metabolic syndrome explodes. Nat Med. 12, 54–55 discussion 55.
Turek, F.W., Joshu, C., Kohsaka, A., Lin, E., Ivanova, G., McDearmon, E., Laposky, A., Losee-Olson, S., Easton, A., Jensen, D.R., Eckel, R.H., Takahashi, J.S., Bass, J., 2005. Obesity and metabolic syndrome in circadian Clock mutant mice. Science 308, 1043–1045.
Uno, K., Katagiri, H., Yamada, T., Ishigaki, Y., Ogihara, T., Imai, J., Hasegawa, Y., Gao, J., Kaneko, K., Iwasaki, H., Ishihara, H., Sasano, H., Inukai, K., Mizuguchi, H., Asano, T., Shiota, M., Nakazato, M., Oka, Y., 2006. Neuronal pathway from the liver modulates energy expenditure and systemic insulin sensitivity. Science 312, 1656–1659.
Yamada, T., Oka, Y., Katagiri, H., 2008. Inter-organ metabolic communication involved in energy homeostasis: potential therapeutic targets for obesity and metabolic syndrome. Pharmacol. Ther. 117, 188–198.

Yamada, T., Katagiri, H., Ishigaki, Y., Ogihara, T., Imai, J., Uno, K., Hasegawa, Y., Gao, J., Ishihara, H., Niijima, A., Mano, H., Aburatani, H., Asano, T., Oka, Y., 2006. Signals fromintra-abdominal fat modulate insulin and leptin sensitivity through different mechanisms: neuronal involvement in food-intake regulation. Cell. Metab. 3, 223–229.

Yang, Q., Graham, T.E., Mody, N., Preitner, F., Peroni, O.D., Zabolotny, J.M., Kotani, K., Quadro, L., Kahn, B.B., 2005. Serum retinol binding protein 4 contributes to insulin resistance in obesity and type 2 diabetes. Nature 436, 356–362.

Yang, X., Downes, M., Yu, R.T., Bookout, A.L., He, W., Straume, M., Mangelsdorf, D.J., Evans, R.M., 2006. Nuclear receptor expression links the circadian clock to metabolism. Cell 126, 801–810.

Neuroscience Research 64 (2009) 213–230

Contents lists available at ScienceDirect

Neuroscience Research

journal homepage: www.elsevier.com/locate/neures

Wolfram syndrome 1 (*Wfs1*) mRNA expression in the normal mouse brain during postnatal development

June Kawano [a,b,*], Ryutaro Fujinaga [b], Kiwako Yamamoto-Hanada [b], Yoshitomo Oka [c,d], Yukio Tanizawa [c], Koh Shinoda [b]

[a] *Laboratory for Neuroanatomy, Department of Neurology, Kagoshima University Graduate School of Medical and Dental Sciences, Kagoshima, 890-8544, Japan*
[b] *Division of Neuroanatomy, Department of Neuroscience, Yamaguchi University School of Medicine, Ube, Yamaguchi, 755-8505, Japan*
[c] *Division of Endocrinology, Metabolism, Hematological Sciences and Therapeutics, Department of Bio-Signal Analysis, Yamaguchi University Graduate School of Medicine, Ube, Yamaguchi, 755-8505, Japan*
[d] *Division of Molecular Metabolism and Diabetes, Tohoku University Graduate School of Medicine, Sendai, Miyagi, 980-8575, Japan*

ARTICLE INFO

Article history:
Received 28 August 2008
Received in revised form 28 February 2009
Accepted 4 March 2009
Available online 20 March 2009

Keywords:
Wolframin
CA1 field
Parasubiculum
Entorhinal cortex
Facial nucleus
Diabetes insipidus
Sensorineural hearing loss
In situ hybridization histochemistry

ABSTRACT

Wolfram syndrome is a rare genetic disorder accompanying diabetes insipidus, sensorineural hearing loss, neurological complications, and psychiatric illness. This syndrome has been attributed to mutations in the *WFS1* gene. In this study, we made a detailed histochemical analysis of the distribution of *Wfs1* mRNA in the brain of developing mice. There were three patterns of change in the strength of *Wfs1* mRNA signals from birth to early adulthood. In type 1, the signals were weak or absent in neonates but strong or moderate in young adults. This pattern was observed in the CA1 field, parasubiculum, and entorhinal cortex. In type 2, the signals were of a relatively constant strength during development. This pattern was seen in limbic structures (e.g. subiculum and central amygdaloid nucleus) and brainstem nuclei (e.g. facial and chochlear nuclei). In type 3, the signals peaked in the second week of age. This pattern was observed in the thalamic reticular nucleus. Thus, *Wfs1* mRNA was widely distributed in the normal mouse brain during postnatal development. This evidence may provide clues as to the physiological role of the *Wfs1* gene in the central nervous system, and help to explain endocrinological, otological, neurological, and psychiatric symptoms in Wolfram syndrome patients.

1. Introduction

Wolfram syndrome (OMIM 222300) is an autosomal recessive neurodegenerative disorder defined by young-onset non-autoimmune insulin-dependent diabetes mellitus and progressive optic atrophy (Wolfram and Wagener, 1938; Minton et al., 2003). The nuclear gene responsible for Wolfram syndrome has been identified as *WFS1* (Wolfram syndrome 1; Inoue et al., 1998; Strom et al., 1998), and is located at 4p16.1 (Polymeropoulos et al., 1994; Collier et al., 1996). The *WFS1* gene is also responsible for autosomal dominant low frequency sensorineural hearing loss (Bespalova et al., 2001; Young et al., 2001), and is a candidate to contribute low risk for type 2 diabetes mellitus (Minton et al., 2002; Sparsø et al., 2008; Wasson and Permutt, 2008). The WFS1 protein, also called wolframin, localizes primarily to the endoplasmic reticulum (ER) membrane, and contains nine transmembrane segments with the amino-terminus in the cytosol and the carboxy-terminus in the ER lumen (Takeda et al., 2001; Hofmann et al., 2003). Subsequent functional studies showed that the WFS1 protein is important in the regulation of intracellular Ca^{2+} homeostasis (Osman et al., 2003; Takei et al., 2006), contributes to cell cycle progression (Yamada et al., 2006), and is produced under conditions of troubled homeostasis, including ER stress (Yamaguchi et al., 2004; Fonseca et al., 2005; Ueda et al., 2005). In addition, screening for mutations in Wolfram syndrome patients demonstrated more than 50 distinct mutations of the *WFS1* gene, including stop, frameshift, deletion and missense mutations (Inoue et al., 1998; Strom et al., 1998; Hardy et al., 1999; Gómez-Zaera et al., 2001; Khanim et al., 2001; Tessa et al., 2001; Cano et al., 2007). Thus loss-of-function mutations in the *WFS1* gene have been linked to Wolfram syndrome, however, molecular functions of the WFS1 protein and the mechanism by which mutations of the *WFS1* gene cause Wolfram syndrome remain unclear.

* Corresponding author at: Laboratory for Neuroanatomy, Department of Neurology, Kagoshima University Graduate School of Medical and Dental Sciences, 35-1, Sakuragaoka 8-chome, Kagoshima, 890-8544, Japan. Tel.: +81 99 275 5212; fax: +81 99 275 5214.
E-mail address: kawanoj@m2.kufm.kagoshima-u.ac.jp (J. Kawano).

0168-0102/$ – see front matter © 2009 Elsevier Ireland Ltd and the Japan Neuroscience Society. All rights reserved.
doi:10.1016/j.neures.2009.03.005

Although the defining characteristics of Wolfram syndrome are diabetes mellitus (100%)[1] and optic atrophy (100%), other symptoms include cranial diabetes insipidus (73%), sensorineural deafness (62%), neurological complications (cerebellar ataxia and myoclonus; 62%), and psychiatric illness (60%) (Swift et al., 1990; Barrett et al., 1995). Accordingly, the term DIDMOAD (diabetes insipidus, diabetes mellitus, optic atrophy, and deafness) is used to describe Wolfram syndrome with more widespread complications (Barrett et al., 1995). The prevalence of Wolfram syndrome is one per 770,000 in the UK population, and the median age at death (commonly central respiratory failure with brainstem atrophy) is 30 years (range 25–49 years) (Barrett et al., 1995). Neuroradiological (Rando et al., 1992; Scolding et al., 1996; Ito et al., 2007) and neuropathological (Genís et al., 1997; Shannon et al., 1999) studies have reported severe atrophy in the brainstem, cerebellum, and optic nerve of Wolfram syndrome patients. Mild atrophy was also observed in the cerebral cortex and hypothalamus. Thus, clinical and pathological facts concerning brain-related (ophthalmological, endocrinological, otological, neurological, and psychiatric) symptoms in Wolfram syndrome have been accumulated. However, the site of pathology for these symptoms remains unclear. To obtain insights into the site of pathology for the symptoms, it is necessary to examine *WFS1* expression in the brain not only at the adult stage, but also at the developmental stages, since there is a possibility that lack of *WFS1* expression during development contributes to the progression of the brain-related symptoms of Wolfram syndrome caused by loss-of-function mutations in the *WFS1* gene. Insights into the site of pathology may provide hypotheses about the pathophysiology of the brain-related symptoms of Wolfram syndrome.

In the rodent brain, expression of the *Wfs1* gene has previously been described in the cerebral cortex, the basal ganglia, the hypothalamus, the brainstem motor and sensory nuclei, the reticular formation, and in the cerebellar cortex, as well as in the CA1 field of the hippocampus and in the amygdala (Takeda et al., 2001; Ishihara et al., 2004; Kato et al., 2008; Kawano et al., 2008; Luuk et al., 2008). To obtain neuroanatomical evidence for understanding the endocrinological, otological, neurological, and psychiatric symptoms of Wolfram syndrome, and to establish a basis for functional studies of the WFS1 protein in the brain, we performed a detailed histochemical analysis of the distribution of *Wfs1* mRNA signals in the brain of normal mice during postnatal development.

2. Materials and methods

2.1. Animals and tissue preparation

Male mice (n = 10; C57BL/6NCrlCrlj; Charles River Laboratories Japan, Inc., Yokohama, Kanagawa, Japan) were used in this study. The delivery day was designated as postnatal day 0 (P0). Three mice at 8 weeks old (P8W, early adulthood), two mice at P28, and five neonates at early postnatal ages, P0, P4, P7, P14, and P21, were used. Prior to the experiments, they were housed in an animal care facility with a 12-h light (lights on 8:00–20:00), 12-h dark photoperiod and free access to tap water and rodent chow. The mice were deeply anesthetized with sodium pentobarbital (50 mg/kg, i.p.), and perfused transcardially with 4% paraformaldehyde dissolved in 0.1 M sodium phosphate buffer (PB; pH 7.4) at 4 °C. Brains were removed from the skull, stored in the same fixative for 48 h, and then immersed in 30% saccharose in 0.1 M PB at 4 °C until they sank. The brains were frozen in powdered dry ice and coronally cut at a thickness of 40 μm. The sections were collected as a 1-in-5 series in a cryoprotectant medium (33.3% saccharose, 1% polyvinylpyrrolidone (K-30), and 33.3% ethylene glycol in 0.067 M sodium phosphate buffer (pH 7.4) containing 0.067% sodium azide; Warr et al., 1981) and stored at −30 °C prior to use. In each experimental case at ages P0 and P4, heads including the brain were processed as described above without decalcification.

All experimental protocols for this study were approved by the committee on the Ethics of Animal Experimentation at Yamaguchi University School of Medicine, and were conducted according to the guidelines for Animal Research of Yamaguchi University School of Medicine and The Law (No. 105) and Notification (No. 6) of the Japanese Government.

2.2. Preparation of cRNA probes

To synthesize a cRNA probe for *in situ* hybridization, a 1548-base fragment of the mouse *Wfs1* cDNA was amplified by RT-PCR, and subcloned into the vector pCR-Blunt (Invitrogen, Carlsbad, CA). The primers used were MOUSE-U2, 5′-T CCG TAC TCT CAC CGA CCT G-3′, and MOUSE L3, 5′-C TCA GGC GGC AGA CAG GAA T-3′. The fragment encoded the 3′-end of the protein-coding region including the stop codon, and occupied 85% of exon 8 where many mutations have been reported in the *WFS1* gene of Wolfram syndrome patients (Inoue et al., 1998; Strom et al., 1998; Hardy et al., 1999; Gómez-Zaera et al., 2001; Khanim et al., 2001; Cano et al., 2007). Two independent clones containing the insert with a different orientation (pCR-clone 19 for sense, pCR-clone 1 for anti-sense) were used. A sense or an anti-sense cRNA probe was obtained by in vitro transcription with a DIG RNA labeling kit (SP6/T7; Roche Diagnostics GmbH, Penzberg, Germany).

2.3. In situ hybridization histochemistry

In situ hybridization histochemistry was carried out as described previously (Kawano et al., 2008). Free-floating sections washed for 5 min in diethylpyrocarbonate-treated phosphate-buffered saline (DEPC-PBS) were pretreated with 0.2 N HCl for 20 min, washed twice for 5 min in DEPC-PBS, and then acetylated in 0.1 M triethanolamine–HCl (pH 8.0) containing 0.25% acetic anhydride for 10 min. Before the hybridization step, sections were washed again twice for 5 min with DEPC-PBS. All pretreatments were performed at 4 °C. Following the pretreatment, sections were preincubated in hybridization buffer (50% deionized-formamide; 10 mM Tris–HCl, pH 7.5; 1 mM EDTA, pH 8.0; 600 mM NaCl; 1× Denhardt's solution; 10% dextran sulfate; 0.25% sodium dodecyl sulfate; and 200 μg/ml yeast tRNA) at 55 °C for 1 h and then hybridized with DIG-labeled anti-sense cRNA probes (0.5 μg/ml; denatured at 95 °C for 5 min and cooled at 4 °C for 5 min shortly before use) in the same buffer at 55 °C for 16 h. After hybridization, the sections were washed with 2× SSC (300 mM NaCl, and 30 mM sodium citrate, pH 7.0) containing 50% formamide at 55 °C for 1 h, rinsed in wash buffer (500 mM NaCl, 10 mM Tris–HCl, pH 8.0, and 1 mM EDTA, pH 8.0) for 10 min and then incubated with RNase A (20 μg/ml; Sigma–Aldrich, St. Louis, MO) in wash buffer at 37 °C for 30 min. After being rinsed in wash buffer again for 10 min, they were soaked in 2× SSC containing 50% formamide and 0.2× SSC containing 50% formamide at 55 °C for 30 min each. To perform the immunoreaction, the sections were blocked in buffer 2 (buffer 1 (150 mM NaCl, and 100 mM Tris–HCl, pH 7.5) containing 2% blocking reagent) at 20 °C for 1 h and then incubated in buffer 2 containing alkaline phosphatase-conjugated sheep anti-DIG antibody (Roche Diagnostics) diluted 1:3000 at 20 °C for 16 h. After two washes in buffer 1 for 10 min, they were rinsed in buffer 3 (100 mM NaCl, 50 mM $MgCl_2$, and 100 mM Tris–HCl, pH 9.5) for 5 min and incubated with NBT/BCIP substrate (1:50; Roche Diagnostics) in buffer 3 at 37 °C for 2–4 h to visualize the immunocomplex. The coloring reaction was stopped with buffer 4 (1 mM EDTA, and 10 mM Tris–HCl, pH 8.0), and the sections were washed in

[1] Percentage in parentheses shows frequency of the feature in Wolfram syndrome patients.

phosphate-buffered saline, mounted on glass slides using a 0.6% gelatin solution, and air-dried. The slides were coverslipped with Entellan neu mountant (Merck KGaA, Darmstadt, Germany). As a control, a sense cRNA probe was used instead of the anti-sense cRNA probe. Few mRNA signals were observed in control sections. For the cytoarchitectonic analysis, adjacent series of brain sections at P0 and P8W (early adulthood) were subjected to Nissl staining by using cresyl violet (acetate) (Merck KGaA).

2.4. Photomicrographs and terminology

Brightfield photomicrographs were taken using a DXM1200 color digital camera (Nikon, Tokyo Japan) equipped with an Optiphot-2 photomicroscope (Nikon). Images were transferred to Adobe Photoshop 6 (Adobe Systems, San Jose, CA), and brightness, contrast, and picture sharpness were adjusted. No other adjustment was made.

The nomenclature used for the different regions of the brain primarily followed that of Paxinos and Franklin (2001).

3. Results

3.1. Changes in the strength of *Wfs1* mRNA expression during postnatal development

Postnatal changes in the strength of *Wfs1* mRNA expression in each of the mouse brain structures are shown in Table 1. A general

Table 1
Postnatal changes in the strength of *Wfs1* mRNA expression in each of the mouse brain structures.

		P0	P4	P7	P14	P28	Early adulthood (P8W)
Type 1a (expression is weak in neonates but strong in young adults)							
CA1	CA1 field of the hippocampus	+	++	++	+++	+++	+++
MEA	Medial entorhinal area	–	+	++	+++	+++	+++
LEA	Lateral entorhinal area	–	+	++	+++	+++	+++
PaS	Parasubiculum	–	–	+++	+++	+++	+++
Type 1b (expression is weak in neonates but moderate in young adults)							
MoCII	Layer II in the motor cortex	–	–	+	++	++	++
CgII	Layer II in the cingulate cortex	–	–	+	++	++	++
Pir	Piriform cortex	+	++	++	++	++	++
LS	Lateral septal nucleus	–	–	+	++	++	++
Acb	Nucleus accumbens	+	++	++	++	++	++
Me5	Mesencephalic trigeminal nucleus	+	+	+	+	+	++
7NM	Medial subdivision of the facial nucleus	+	+	+	+	++	++
Amb	Nucleus ambiguus	+	+	+	+	+	++
Type 1c (expression is absent in neonates but weak in young adults)							
SoCII	Layer II in the somatosensory cortex	–	–	–	+	+	+
AuCII	Layer II in the auditory cortex	–	–	–	+	+	+
ViCII	Layer II in the visual cortex	–	–	–	+	+	+
SC	Superior colliculus	–	–	–	+	+	+
Type 2a (expression is moderate and relatively constant throughout postnatal stages)							
S	Subiculum	++	++	++	++	++	++
Tu	Olfactory tuberculum	++	++	++	++	++	++
BSTL	Lateral bed nucleus of the stria terminalis	++	++	++	++	++	++
IPAC	Interstitial nucleus of the posterior limb of the anterior commissure	++	++	++	++	++	++
Ce	Central amygdaloid nucleus	++	++	++	++	++	++
CPu	Caudate putamen (caudal part)	++	++	++	++	++	++
Mo5	Motor nucleus of the trigeminal nerve	++	++	++	++	++	++
7NL	Lateral subdivision of the facial nucleus	++	++	++	++	++	++
12N	Hypoglossal nucleus	++	++	++	++	++	++
Type 2b (expression is weak and relatively constant throughout postnatal stages)							
MOB	Main olfactory bulb	+	+	+	+	+	+
AOB	Accessory olfactory bulb	+	+	+	+	+	+
SO	Supraoptic nucleus	+	+	+	+	+	+
PVNm	Magnocellular part of the paraventricular hypothalamic nucleus	+	+	+	+	+	+
IC	Inferior colliculus	+	+	+	+	+	+
LC	Nucleus coeruleus	+	+	+	+	+	+
DR	Dorsal raphe nucleus	+	+	+	+	+	+
MnR	Median raphe nucleus	+	+	+	+	+	+
Co	Cochlear nucleus	+	+	+	+	+	+
BSRt	Brainstem reticular formation	+	+	+	+	+	+
Pur	Purkinje cell layer of the cerebellar cortex	–	+	+	+	+	+
Type 3a (peak expression is moderate, and seen in the second week of age)							
Rt	Thalamic reticular nucleus	+	+	++	++	+	+
Type 3b (peak expression is weak, and seen in the second week of age)							
MoCV	Layer V in the motor cortex	–	–	+	+	–	–
SoCV	Layer V in the somatosensory cortex	–	–	+	+	–	–
AuCV	Layer V in the auditory cortex	–	–	+	+	–	–
ViCV	Layer V in the visual cortex	–	–	+	+	–	–
CgV	Layer V in the cingulate cortex	–	+	+	+	–	–
RSCII	Layer II in the retrosplenial cortex	–	–	+	+	–	–
RSCV	Layer V in the retrosplenial cortex	+	+	+	+	–	–

+++, strong expression; ++, moderate expression; +, weak expression; –, undetectable expression.
P0, P4, P7, P14, P28, and P8W indicate postnatal days 0, 4, 7, 14, and 28, and postnatal week 8, respectively.
Abbreviations of the nomenclature are described in the far left column.

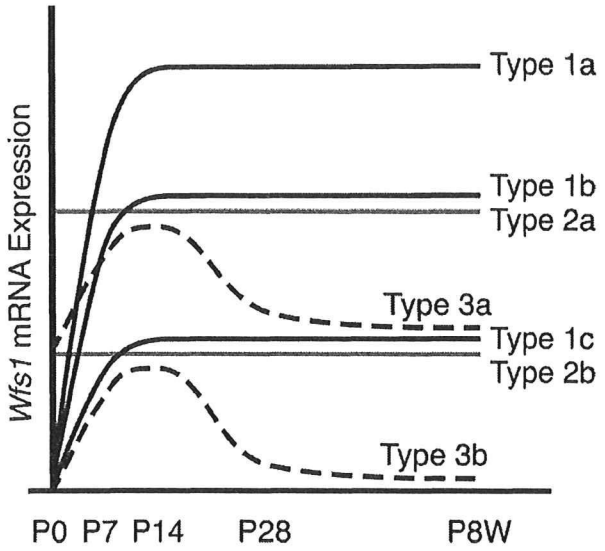

Fig. 1. A graph showing a general impression of postnatal changes in the strength of *Wfs1* mRNA expression in each structure of the mouse brain. Black-solid, shaded-solid, and black-dashed lines indicate types 1, 2, and 3 patterns, respectively. Upper part of the graph represents stronger *Wfs1* mRNA expression. P0, P7, P14, P28, and P8W show postnatal days 0, 7, 14, and 28, and postnatal week 8, respectively. Note that the patterns are categorized into three types. In addition, each type is classified into two or three subtypes (e.g. 1a, 1b, and 1c) according to the maximum strength of *Wfs1* mRNA expression during postnatal development.

impression of the changes is provided in Fig. 1, which shows a graph, depicting patterns of change in the strength of *Wfs1* mRNA expression from birth to early adulthood. As shown in Fig. 1, the patterns were classified into three types (1, 2, and 3) according to the strength of *Wfs1* mRNA expression at different developmental stages. In the type 1 pattern, *Wfs1* mRNA signals were weak or absent on delivery day (P0), progressively increased from P0 to postnatal day 14 (P14), and were of a relatively stable strength from P14 to early adulthood (postnatal week 8; P8W). In addition, type 1 was categorized into three subtypes (1a, 1b, and 1c) according to the strength of *Wfs1* mRNA expression from P14 to early adulthood (P8W). In type 1a, strong *Wfs1* mRNA signals were seen from P14 to early adulthood (P8W). This pattern was observed in the CA1 field of the hippocampus (CA1), the medial entorhinal area (MEA), the lateral entorhinal area (LEA), and in the parasubiculum (PaS) (Figs. 1 and 2; Table 1). In type 1b, moderate *Wfs1* mRNA signals were seen from P14 to early adulthood (P8W). This pattern was observed in layer II of the motor (MoCII) and cingulate (CgII) cortices, the piriform cortex (Pir), the lateral septal nucleus (LS), nucleus accumbens (Acb), the mesencephalic trigeminal nucleus (Me5), the medial subdivision of the facial nucleus (7NM), and in nucleus ambiguus (Amb) (Figs. 1, 3, 4G–L; Table 1). In type 1c, weak *Wfs1* mRNA signals were seen from P14 to early adulthood (P8W). This pattern was observed in layer II of the somatosensory (SoCII), auditory (AuCII) and visual (ViCII) cortices, and in the superior colliculus (SC) (Fig. 1; Table 1).

In the type 2 pattern, *Wfs1* mRNA signals were of a relatively constant strength from P0 to early adulthood (P8W). Like type 1,

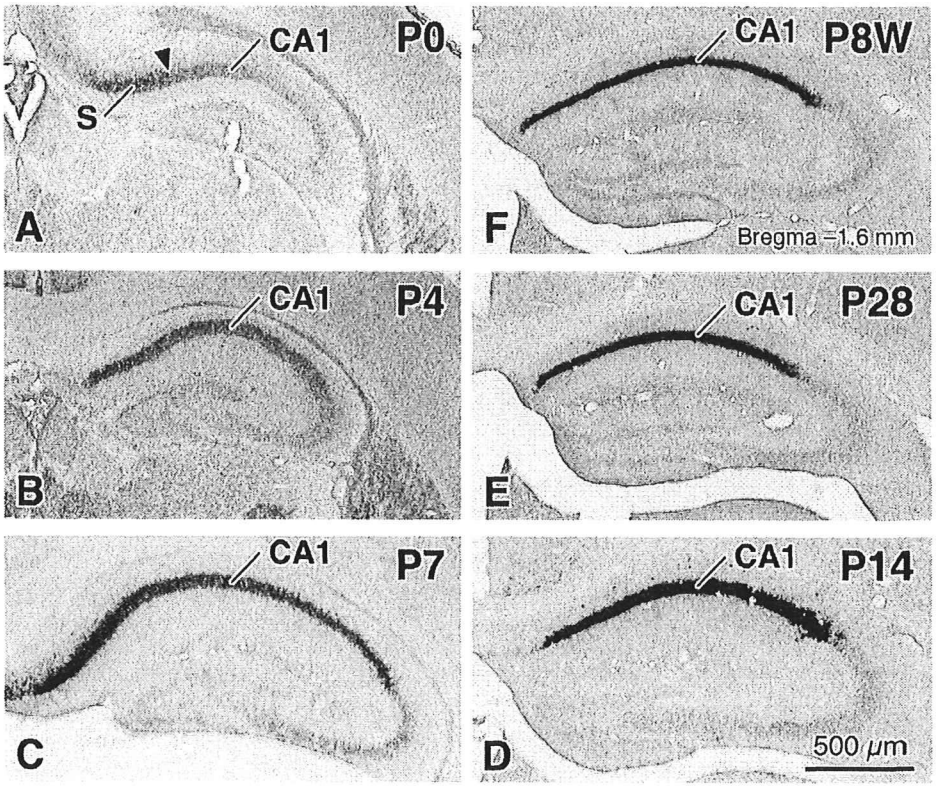

Fig. 2. Type 1a pattern of *Wfs1* mRNA signals in the mouse brain during postnatal development. (A–F) Changes in *Wfs1* mRNA signals in the CA1 field of the hippocampus (CA1) during postnatal development. The day of birth is regarded as postnatal day 0 (P0). P4, P7, P14, P28, and P8W indicate postnatal days 4, 7, 14, and 28, and postnatal week 8, respectively. Brain sections of P0, P4, P7, P14, P28, and of P8W mice are shown in panels (A), (B), (C), (D), (E), and (F), respectively. The arrowhead in (A) shows the border between the subiculum (S) and the CA1 field. The bregma level of a P8W-mouse section is represented at the lower right in (F). Scale bar = 500 μm in (D) for (A–C) and for (E and F). (G–L) Changes in *Wfs1* mRNA signals in the parasubiculum (PaS) and the medial entorhinal area (MEA) during postnatal development. Brain sections of P0, P4, P7, P14, P28, and of P8W mice are shown in panels (G), (H), (I), (J), (K), and (L), respectively. Arrowheads in (H–L) show the boundary between the PaS and the MEA. The bregma level of a P8W-mouse section is represented at the lower right in (L). Note that *Wfs1* mRNA signals in the type 1a pattern are weak or absent on P0, progressively increase from P0 to P14, are strong on P14, and are of a relatively stable strength from P14 to P8W. LEA, lateral entorhinal area. Scale bar = 500 μm in (J) for (G–I) and for (K and L).

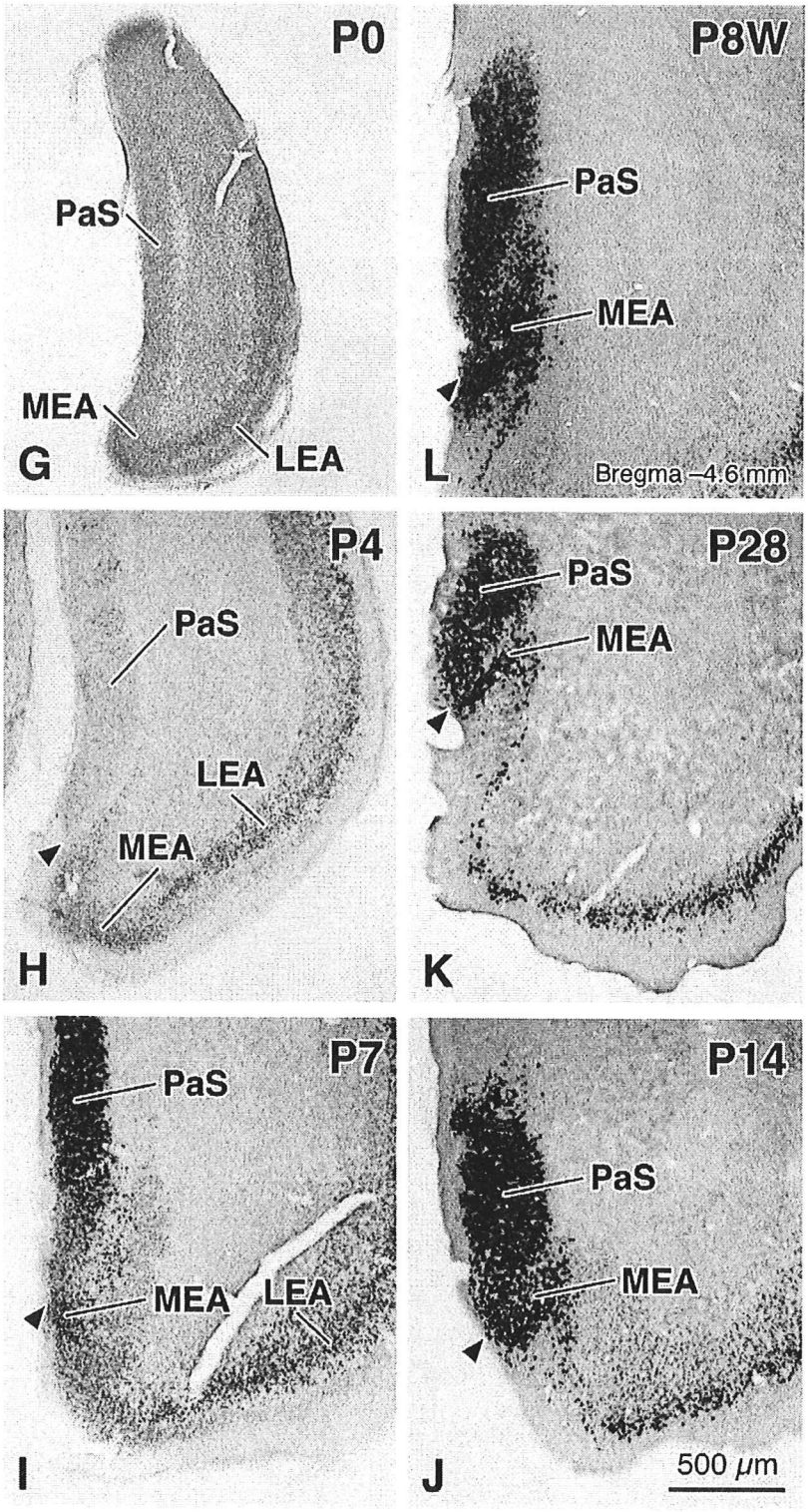

Fig. 2. (*Continued*).

type 2 was categorized into two subtypes (2a and 2b) according to the strength of *Wfs1* mRNA expression from P0 to early adulthood (P8W). In type 2a, moderate *Wfs1* mRNA signals were invariably seen. This pattern was mainly observed in the limbic structures, and in the brainstem motor nuclei. It was found in the subiculum (S), the olfactory tuberculum (Tu), the lateral bed nucleus of the stria terminalis (BSTL), the interstitial nucleus of the posterior limb of the anterior commissure (IPAC), the central amygdaloid nucleus (Ce), the caudal part of the caudate putamen (CPu), the motor nucleus of the trigeminal nerve (Mo5), the lateral subdivision of the facial nucleus (7NL), and in the hypoglossal nucleus (12N) (Figs. 1 and 4; Table 1). As described above, in the facial nucleus,

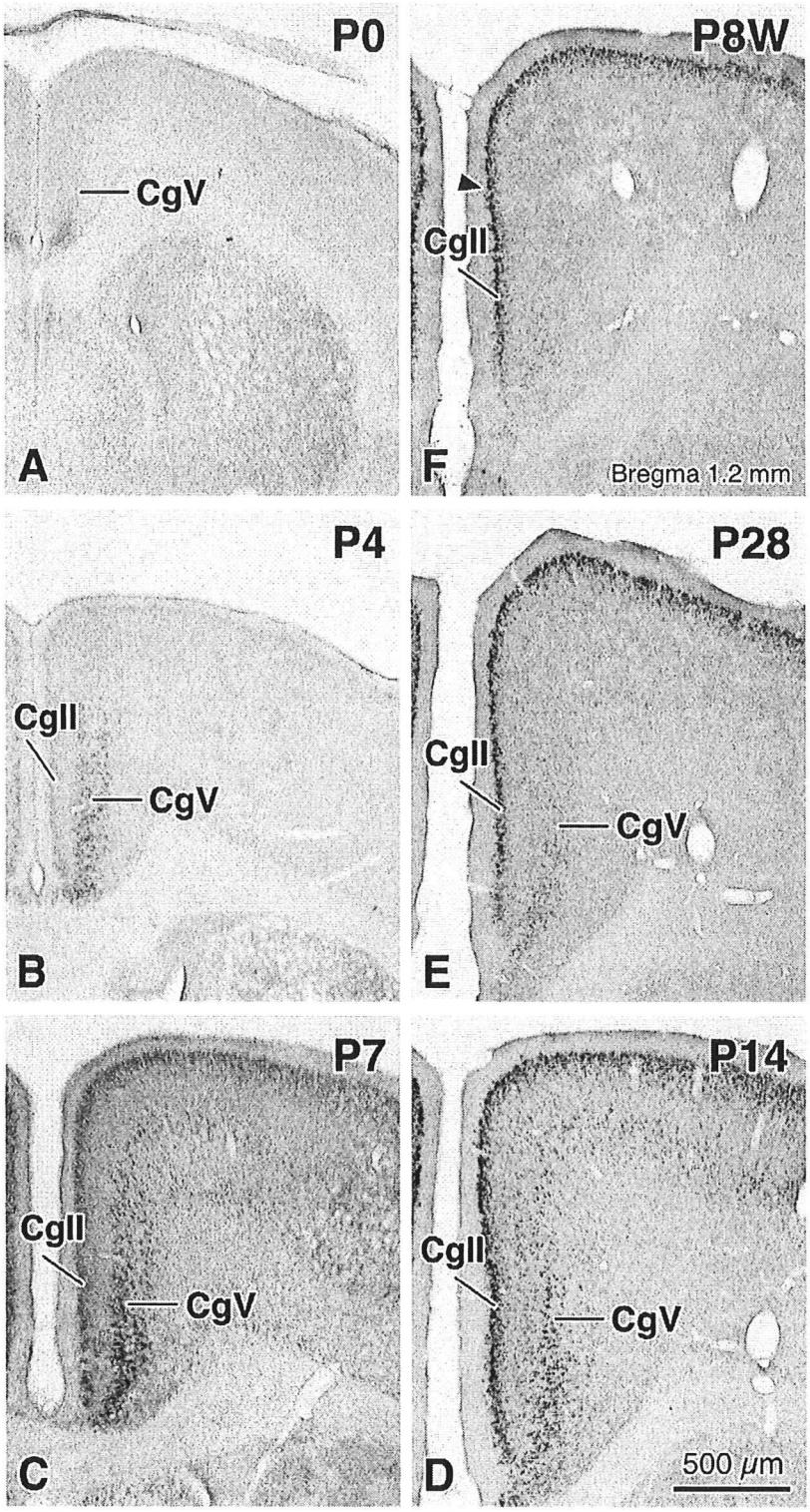

Fig. 3. Type 1b pattern of *Wfs1* mRNA signals in the mouse brain during postnatal development. (A–F) Changes in *Wfs1* mRNA signals in layer II of the cingulate cortex (CgII) during postnatal development. The day of birth is regarded as postnatal day 0 (P0). P4, P7, P14, P28, and P8W indicate postnatal days 4, 7, 14, and 28, and postnatal week 8, respectively. Brain sections of P0, P4, P7, P14, P28, and of P8W mice are shown in panels (A), (B), (C), (D), (E), and (F), respectively. The arrowhead in (F) shows the border between the cingulate cortex and the motor cortex. The bregma level of a P8W-mouse section is represented at the lower right in (F). A type 3b pattern is seen in layer V of the cingulate cortex (CgV). Scale bar = 500 μm in (D) for (A–C) and for (E and F). (G–L) Changes in *Wfs1* mRNA signals in the lateral septal nucleus (LS) during postnatal development. Brain sections of P0, P4, P7, P14, P28, and of P8W mice are shown in panels (G), (H), (I), (J), (K), and (L), respectively. The bregma level of a P8W-mouse section is represented at the lower right in (L). Note that *Wfs1* mRNA signals in the type 1b pattern are weak or absent on P0, progressively increase from P0 to P14, are moderate on P14, and are of a relatively stable strength from P14 to P8W. CPu, caudate putamen. Scale bar = 500 μm in (J) for (G–I) and for (K and L).